CANADIAN JOURNAL OF RESEARCH

VOLUME 28 SEPTEMBER, 1950 NUMBER 5

— SECTION A —

PHYSICAL SCIENCES

Contents

Page

Gamma-ray Studies Using Deuterium-loaded Photographic Plates—*C. H. Millar, A. G. W. Cameron, and M. Glicksman* 475

Two New $^1\Sigma - ^1\Sigma$ Systems Due to the Molecule NO — *M. W. Feast* - 488

Energy Distribution of Fission Fragments from Pu^{239}—*D. C. Brunton and W. B. Thompson* - - - - - - - - - - - 498

The Velocity of Sound in Helium at Temperatures −78°C. to 200°C. and Pressures up to 70 Atmospheres — *W. G. Schneider and G. J. Thiessen* - - - - - - - - - - - 509

A Calorimetric Measurement of the Disintegration Rate of a P^{32} Source—*J. G. Bayly* - - - - - - - - - - - - - 520

Continuous Observations with the Electron Microscope on the Formation of Evaporated Films of Silver, Gold, and Tin—*T. A. McLauchlan, R. S. Sennett, and G. D. Scott* - - - 530

Measurements of Gravity in the Canadian Arctic and Greenland—*Michael Beer* - - - - - - - - - - - - - - - 535

Probability of Auto-ionization in Light Atoms—*Ta-You Wu and Lorraine Ourom* - - - - - - - - - - - - - - - 542

NATIONAL RESEARCH COUNCIL
OTTAWA, CANADA

CANADIAN JOURNAL OF RESEARCH

The *Canadian Journal of Research* is issued in six sections, as follows:

A. Physical Sciences	D. Zoological Sciences
B. Chemical Sciences	E. Medical Sciences
C. Botanical Sciences	F. Technology

For the present, Sections A, C, D, and E are to be issued six times annually, and Sections B and F, twelve times annually, each under separate cover, with separate pagination.

The *Canadian Journal of Research* is published by the National Research Council of Canada under authority of the Chairman of the Committee of the Privy Council on Scientific and Industrial Research. The *Canadian Journal of Research* is edited by a joint Editorial Board consisting of members of the National Research Council of Canada, the Royal Society of Canada, and the Chemical Institute of Canada.

Sections B and F of the *Canadian Journal of Research* have been chosen by the Chemical Institute of Canada as its medium of publication for scientific papers.

EDITORIAL BOARD

Representing
NATIONAL RESEARCH COUNCIL

DR. H. P. ARMES (*Chairman*),
Dean of the University,
University of Manitoba,
Winnipeg, Man.

DR. OTTO MAASS,
Macdonald Professor of Physical Chemistry,
McGill University,
Montreal, P.Q.

DR. J. H. L. JOHNSTONE,
Professor of Physics,
Dalhousie University,
Halifax, N.S.

DR. A. BERTRAND,
Professor of Bacteriology,
Faculty of Medicine,
University of Montreal,
Montreal, P.Q.

Representing
ROYAL SOCIETY OF CANADA

DR. G. M. VOLKOFF,
Professor of Physics,
University of British Columbia,
Vancouver, B.C.
} Section III

DR. J. W. T. SPINKS,
Dean, College of Graduate Studies,
University of Saskatchewan,
Saskatoon.
} Section III

DR. H. S. JACKSON,
Head, Department of Botany,
University of Toronto,
Toronto.

DR. E. HORNE CRAIGIE,
Department of Zoology,
University of Toronto,
Toronto.
} Section V

Ex officio

DR. LÉO MARION, Editor-in-Chief,
Division of Chemistry,
National Research Laboratories,
Ottawa.

DR. H. H. SAUNDERSON,
Director, Division of Information Services,
National Research Council,
Ottawa.

Representing
THE CHEMICAL INSTITUTE OF CANADA

DR. H. G. THODE,
Department of Chemistry,
McMaster University,
Hamilton.

EDITORIAL COMMITTEE

Editor-in-Chief,	DR. LÉO MARION	Editor, Section D,	DR. E. HORNE CRAIGIE
Editor, Section A,	DR. G. M. VOLKOFF	Editor, Section E,	DR. J. B. COLLIP
Editor, Section B,	DR. J. W. T. SPINKS DR. H. G. THODE	Editor, Section F,	DR. J. A. ANDERSON DR. G. M. VOLKOFF DR. H. G. THODE
Editor, Section C,	DR. H. S. JACKSON		

Manuscripts should be addressed:

Editor-in-Chief,
Canadian Journal of Research,
National Research Council, Ottawa, Canada.

NOTICE

The Canadian Journal of Research is at present published in six sections, A to F. Starting with January 1, 1951, these sections will be published as separate journals under distinctive names and the designation Canadian Journal of Research will no longer be used. The present names and the corresponding new names are as follows:

Present Name	*New Name*
Canadian Journal of Research, Section A (Physical Sciences)	Canadian Journal of Physics
Canadian Journal of Research, Section B (Chemical Sciences)	Canadian Journal of Chemistry
Canadian Journal of Research, Section C (Botanical Sciences)	Canadian Journal of Botany
Canadian Journal of Research, Section D (Zoological Sciences)	Canadian Journal of Zoology
Canadian Journal of Research, Section E (Medical Sciences)	Canadian Journal of Medical Sciences
Canadian Journal of Research, Section F (Technological Sciences)	Canadian Journal of Technology

In order to preserve continuity the present sequence of volume numbers will be retained, and in each case the volume for 1951 will be Volume 29.

The subscription rates for the Journals will remain as at present.

Canadian Journal of Research

Issued by THE NATIONAL RESEARCH COUNCIL OF CANADA

VOL. 28, SEC. A. SEPTEMBER, 1950 NUMBER 5

GAMMA-RAY STUDIES USING DEUTERIUM-LOADED PHOTOGRAPHIC PLATES[1]

BY C. H. MILLAR, A. G. W. CAMERON, AND M. GLICKSMAN[2]

Abstract

Deuterium-loaded nuclear emulsions have been used to study the γ-rays of neutron capture in sodium, chlorine, and cadmium, and the γ-rays following the β-decay of N^{16}. Proton tracks caused by the photodisintegration of deuterium were measured, and from these the γ-ray energies were calculated. Several lines have been observed in the γ-ray spectra of neutron capture. The known energy of the 6.124 Mev. γ-ray following the decay of N^{16} (produced in the cooling water of the Chalk River pile) was used to calibrate the plates. A higher energy γ-ray from the decay of N^{16} was tentatively identified as corresponding to a transition from the 6.897 Mev. excited level of O^{16} to the ground state and was found to have one-seventh the intensity of the 6.124 Mev. γ-ray.

I. Introduction

High energy γ-rays may be studied by allowing them to impinge on a nuclear research emulsion loaded with deuterium. A γ-ray whose energy exceeds the binding energy of the deuteron may cause its photodisintegration, and, from the range and direction of the photo-proton track thus produced in the emulsion, the energy of the γ-ray may be calculated.

Gibson, Green, and Livesey (5) studied the angular distribution of the γ-rays from the reaction $F^{19}(p, \alpha)O^{16*}$, using a nuclear research emulsion loaded with $Ca(NO_3)_2$ having D_2O as water of crystallization. Such emulsions, though satisfactory when fresh, lose their deuterium by exchange of hydrogen quite rapidly. Goldhaber (6) studied the γ-ray energies from this same reaction, and Hamermesh (7) studied the γ-rays of neutron capture in cadmium, using ordinary nuclear research emulsions soaked in D_2O. While a large quantity of deuterium is incorporated into the emulsion by this procedure, the emulsion is partly desensitized and the range–energy relation is changed by an amount that is difficult to keep constant, since the emulsion swells rapidly when first soaked and continues to swell slowly for several hours during soaking.

We were fortunate in obtaining some plates coated with a specially prepared Ilford type C2 emulsion, nominally 115 microns in thickness, containing 0.40 mgm. per cm.^{2} of deuterium incorporated in the stable organic compound hexadeutero diacetin. With these plates we have obtained some information

[1] *Manuscript received May 9, 1950.*
Contribution from the Nuclear Physics Branch, Atomic Energy Project, National Research Council of Canada, Chalk River, Ont. Issued as N.R.C. No. 2181.

[2] *Now at the University of Chicago, Chicago, Illinois, U.S.A.*

on the spectra of γ-rays following neutron capture in sodium, chlorine, and cadmium and also on the γ-rays following the decay of N^{16} to excited states of O^{16}.

II. γ-Rays of Neutron Capture in Sodium, Chlorine, and Cadmium

(*a*) *Experimental Procedure*

The experimental arrangement for studying γ-rays of neutron capture is shown in Fig. 1. A collimated beam of neutrons from the thermal column of the Chalk River pile struck the 3-in.-square sample of the substance under study. In the case of sodium the source was pure metal, 1 in. thick, wrapped in 0.002 in. aluminum sheet; chlorine was irradiated in the form of a 1/2 in. thickness of anhydrous magnesium chloride powder held in a container of

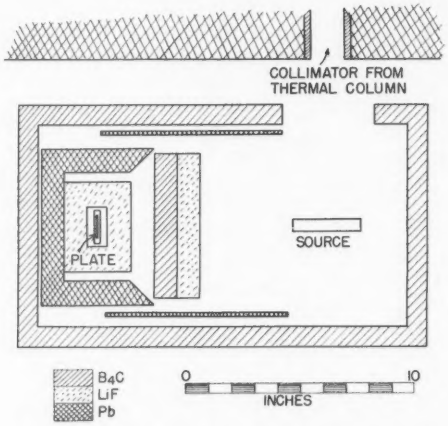

FIG. 1. *Schematic diagram of apparatus used for irradiating photographic plates with γ-rays of neutron capture at the thermal column of the NRX pile.*

similar aluminum sheet; and cadmium sheet 0.015 in. thick was used in the third case.

The γ-rays of neutron capture, emitted at right angles to the neutron beam, passed through the lithium fluoride and boron carbide neutron shields with little probability of energy degradation, and entered the nuclear research emulsion. This was set normally to the beam in order that the $\sin^2\theta$ angular distribution (15) of the photo-protons would favor the production of proton tracks in the plane of the emulsion. The undeflected and scattered neutrons were in general captured by the boron carbide within the double walls of the box containing the equipment, giving rise to γ-rays below the threshold for the photo-disintegration of deuterium. A large percentage of these γ-rays were prevented from reaching the plate (and causing unwanted fogging) by the lead shields disposed about the box. Neutron shielding immediately around the

plate and between the plate and the target was effected to as large an extent as possible by lithium fluoride, which emits no appreciable γ-rays of neutron capture but is less efficient than boron carbide as a neutron shield. In the case of cadmium, where nearly all of the neutrons were captured by the foil, the lithium fluoride and boron carbide absorbers between the source and the plate holder were omitted. Irradiations were carried out until the plates had the maximum tolerable γ-ray fogging that would allow the accurate detection and measurement of proton tracks.

The plates were developed for 15 min. in a rocking bath of one-quarter strength Kodak D-19, after which they were immersed in a 2% acetic acid stop bath for five minutes, and finally fixed in Kodak Acid Fixer for approximately one hour. The search for and measurement of tracks was carried out on binocular research microscopes of a nominal magnification of 1687 diameters. It was found that about 350 tracks per cm.^{2} could be obtained under good conditions—that is, where appreciable parts of the γ-ray spectrum had suitably large cross sections for the photodisintegration of deuterium.

(*b*) *Treatment of Data*

Preliminary range–energy calibration of these special emulsions, by measurement of four-pronged α-particle stars arising from the successive disintegrations of Ra^{226}, a natural contaminant, showed that ranges were somewhat greater than those expected from the range–energy relationship of Lattes, Fowler, and Cuer (9). However, accurate calibration was ultimately carried out by means of the principal high energy γ-ray following the β-decay of N^{16}, the study of which is described in Section III. A rough value of 6.2 Mev. was found for this γ-ray and from this it was assumed that it arose from the transition to the ground state from the 6.124 Mev. level in O^{16}(4). A correction factor was applied to the data to adjust the peak of the photo-proton histogram to correspond to this figure. This calibration indicated that there was a 10.5% increase in range for a proton of a given energy over the value obtained from the published range–energy relationship (9) for standard Ilford C2 emulsion, and a corrected range–energy relationship based upon this factor was accordingly drawn up and used throughout this work.

From the photo-proton energies as determined by the modified range–energy relationship, the corresponding γ-ray energies were computed from the equation:

$$E_\gamma = 2E_p + Q + \epsilon,$$

where E_γ is the energy (Mev.) of the photon, E_p is the photo-proton energy (Mev.), Q is the binding energy of the deuteron = 2.24 Mev. (1), and ϵ is a small angular-dependent energy correction term. A close approximation for ϵ is obtained from the equation:

$$\epsilon = \frac{E_\gamma^2}{1880} - E_\gamma \cos\theta\left[\frac{E_\gamma - Q}{940}\right]^{1/2},$$

where θ is the angle between the photo-proton and the direction of the incident γ-ray, and E_γ is approximated by $2E_p + Q$.

Histograms were plotted of the resulting γ-ray spectra, and these distributions were then corrected for (1) the escape of protons from the emulsion, (2) the variation in the cross section for the photodisintegration of the deuteron, and (3) the background tracks in the emulsion.

The escape-correction factor, C_e, is the ratio of all photo-proton tracks originating in the emulsion to those that do not escape. By taking into account the $\sin^2\theta$ distribution of the photo-proton tracks and the orientation of the plates, the following expressions are obtained:

$$C_e = \frac{1}{1 - \frac{3}{8}\frac{L}{t}} \text{ for } L \leqslant t,$$

and

$$C_e = \frac{1}{\frac{3}{4}\frac{t}{L} - \frac{1}{8}\left(\frac{t}{L}\right)^3} \text{ for } L > t.$$

Here L is the average length of the photo-proton tracks at the γ-ray energy for which C_e is being calculated, and t is the thickness of the emulsion less 10 microns allowance for tracks ending within 5 microns of either surface since these appear to escape and are therefore rejected.

The cross section correction factor, C_σ, is defined as the ratio of the photodisintegration cross section at $E_\gamma = 2Q$ (where it is a maximum) to the cross section at the energy for which C_σ is being calculated. For the evaluation of C_σ the theoretical curve of Pais (14), calculated on the assumption that the 300 m_e meson is responsible for nuclear forces, was used as reproduced by Rosenfeld (15, pp. 175-179).*

The total correction factor, C, is then:

$$C = C_e C_\sigma,$$

and the ordinates of the γ-ray energy histograms were multiplied by factors taken from the correction factor versus energy curve computed in this manner. The form of this curve was slightly different for each plate used, since the thickness of the emulsion varied among the different plates although it was fairly constant on any one plate.

There were four possible sources of background tracks in the plates. (1) The emulsions had a fairly large number of natural α-particle tracks. This number

** Recent work by Bethe and Longmire (Phys. Rev. 77: 647. 1950) indicates that the photodisintegration cross section of the deuteron is greater near the threshold and at high energies than predicted by Pais. On the basis of this newer theory the intensities of the spectra should be lowered on both sides of 4.5 Mev., the point of normalization. This correction amounts to 14% at 3 and 9 Mev., the extremes of the spectra studied, and is not sufficient to alter line positions appreciably.*

presumably remained constant, since the plates were sufficiently old that an equilibrium was set up between the tracks fading and those being newly formed by radioactive contaminants in the emulsion. Multi-pronged α-particle stars from radium and thorium could be easily recognized and rejected; but there were some single α-particle tracks from substances with long lived descendants and some from ordinary star-producing contaminants in which intermediate daughter nuclei had migrated from their normal positions in the stars before decaying. Newly formed single α-particle tracks could be distinguished from proton tracks because of their greater density, but faded α-particle tracks were indistinguishable from proton tracks. (2) Scattered fast neutrons could "knock-on" hydrogen atoms in the emulsion giving a broad spectrum of proton tracks. (3) Slow neutrons could cause (n, p) reactions in the nitrogen of the emulsion, giving a peak at an apparent γ-ray energy of 3.6 Mev. (4) Photo-proton tracks could arise from γ-rays of neutron capture in the various parts of the apparatus other than the target.

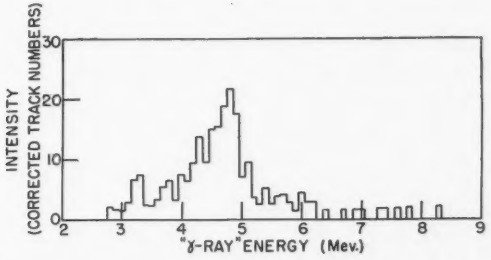

FIG. 2. *Histogram showing a typical background spectrum for γ-rays of neutron capture irradiations. This has been corrected for escape of tracks and "cross section".*

The background was determined experimentally by replacing the neutron capturing sources by a sheet of polystyrene whose thickness was calculated to give an equivalent amount of neutron scattering, and, after a comparable exposure of a "background" plate, an equal volume of emulsion was searched for tracks. Those found were treated as photo-proton tracks and a background "γ-ray energy" histogram computed, which was corrected for escape and "cross section" as before. Such a histogram is shown in Fig. 2. The main peak in the region 4–5 Mev. is due to the background α-particle tracks (see Fig. 8). Fortunately the remaining neutron-produced background was found to be low. The numbers in this distribution were adjusted in the ratio of the volumes searched, and were subtracted from the γ-ray energy distributions as measured for chlorine, cadmium, and sodium.

The resulting histograms are shown in Figs. 4, 5, and 6. The dotted lines show the total corrected distributions obtained while the solid lines show the final results after background has been subtracted.

(*c*) *Resolving Power of the Method*

In order to interpret the γ-ray spectra it is necessary to consider the resolving power of the method. There are four principal uncertainties which contribute to the apparent energy-spread of a mono-energetic γ-ray line measured in this manner. There are the uncertainties in (1) the measurement of the horizontal projection of the track length, (2) the measurement of the vertical projection of the track length, (3) the measured value of the shrinkage factor for the emulsion, and (4) the natural straggling of proton tracks. (The uncertainty of the angle between the incident photon and the photon-proton track is of the second order and may be neglected.)

Since the absolute magnitudes of these various uncertainties are difficult to estimate, we have considered it more accurate to derive the general formula for the half-width* of a γ-ray line and to evaluate its constants in terms of the half-widths found in this experiment.

For a given proton energy the associated proton range, R, is given by

$$R = s\,[a^2 + (bf)^2]^{1/2},$$

where a is the measured horizontal projection, b is the measured vertical projection, f is the shrinkage factor for the emulsion, and s is a straggling factor with a mean value of unity.

From statistical theory it follows (10, p. 498) that:

$$\Delta R = \left[\left(\frac{as^2\Delta a}{R}\right)^2 + \left(\frac{bf^2s^2\Delta b}{R}\right)^2 + \left(\frac{b^2fs^2\Delta f}{R}\right)^2 + \left(\frac{R\Delta s}{s}\right)^2\right]^{1/2},$$

where ΔR is the half-width in range of photo-protons, and Δa, Δb, Δf, and Δs are the partial half-widths of the various parameters. Assuming that s is unity and that Δa, Δb, Δf, and Δs are constant over the range of the experiment, we obtain the approximation

$$\Delta R \doteqdot \left[\left(C_1\frac{a}{R}\right)^2 + \left(C_2\frac{b}{R}\right)^2 + \left(C_3\frac{b^2}{R}\right)^2 + (C_4R)^2\right]^{1/2}.$$

From the complex angular distribution of the proton tracks average values of a and b may be calculated, and these are found to be proportional to R. Therefore the factors a/R and b/R are constant, and the equation reduces to

$$\Delta R \doteqdot [K_1 + K_2R^2]^{1/2}.$$

The constants K_1 and K_2 may be evaluated by means of the experimental values determined for the 6.124 Mev. γ-ray line from the decay of N^{16}(Fig. 9) and the 2.76 Mev. γ-ray line from Na^{24}(Fig. 6). In the case of the N^{16} line, analysis by the method of moments gives a half-width of 0.565 Mev. In the case of Na^{24} the exact measurement of energy half-width is difficult since the corresponding proton tracks are extremely short, and there is a superimposed spectrum of γ-rays of neutron capture which constitute an unknown

*Width of line at half-maximum.

background; however, an estimate of the energy half-width of the 2.76 Mev. line is 0.15 Mev.

Fig. 3 shows the variation of energy half-width with energy computed by means of this method of analysis and fitted to the two experimental points.

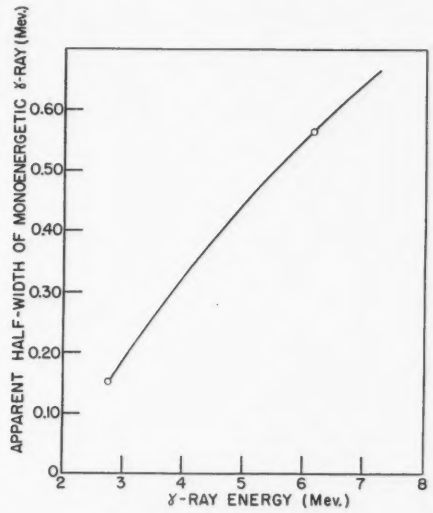

FIG. 3. *Graph showing variation of half-width (width of line at half-maximum) with energy of the γ-ray. The resolving power of the deuterium-loaded plate as a γ-ray spectrometer is thereby indicated.*

(d) Experimental Results

Fig. 4 is a histogram of the γ-rays of neutron capture in $MgCl_2$. Most of this spectrum is probably due to decay from excited levels of Cl^{36} since the thermal neutron capture cross section of Cl^{35} is much larger than that of Cl^{37} or of magnesium (3, 13). The principal feature is the broad peak in the 4.5 to 5.0 Mev. region, which, from consideration of resolving power of the method, must be composed of at least two γ-rays of comparable intensity. There are also indications of peaks at 3.1, 3.4, and 3.9 Mev. but their intensities are too low for complete resolution or accurate measurement of energies.

Shrader and Pollard (16) have found energy levels at 0.96 and 4.81 Mev. in Cl^{36}, and from mass excess considerations the absorption of a thermal neutron by Cl^{35} will produce a Cl^{36} nucleus with an excitation of 8.31 Mev. Table I shows a comparison of observed values with possible γ-ray energies following neutron capture in Cl^{35}, assuming all possible combinations of decay via these known levels.

TABLE I

COMPARISON OF OBSERVED PEAKS IN CAPTURE γ-RAY SPECTRUM OF CHLORINE WITH POSSIBLE OBSERVABLE γ-RAYS CALCULATED FROM ENERGY LEVEL SCHEME OF Cl^{36}

Calculated γ-ray energies, Mev.	Observed γ-ray peaks, Mev.
—	3.1
3.50	3.4
3.85	3.9
4.81	4.5 to 5.0 } Two or more
—	
7.35	—
8.31	—

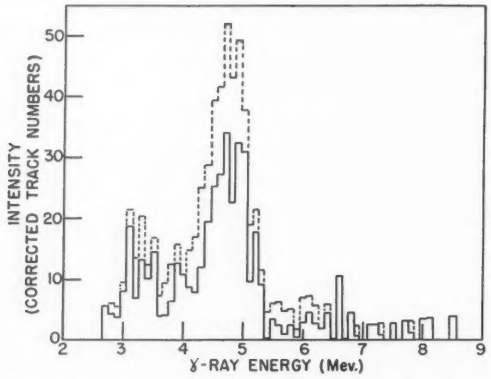

FIG. 4. *Histogram showing the energy distribution of γ-rays of neutron capture in chlorine. Dotted line shows the full spectrum obtained; solid line is the final result after subtraction of background.*

Fig. 5 is a histogram of the γ-rays of neutron capture in cadmium. In general there is no clearly defined structure, though there is some indication of a broad peak in the 5 Mev. region in agreement with the work of Moak and Dabbs (11).

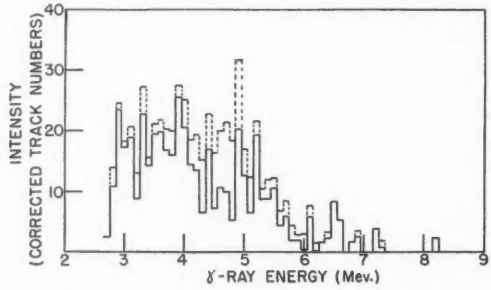

FIG. 5. *Histogram showing the energy distribution of γ-rays of neutron capture in cadmium. Dotted line shows the full spectrum obtained; solid line is the final result after subtraction of background.*

There is also an apparent peak at 3.0 Mev. The over-all picture, however, is of an unresolved spectrum decreasing steadily from a maximum at the lower energy limit of the observations up to about 7.5 Mev.

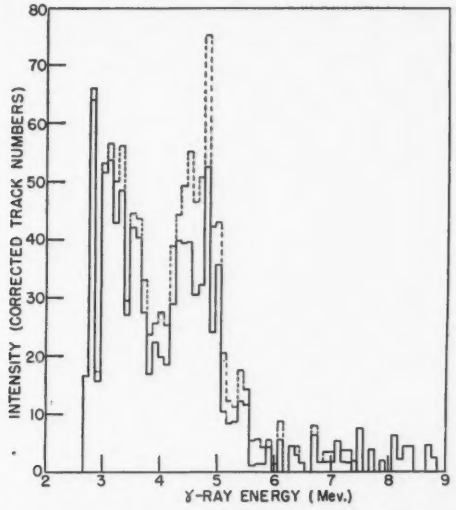

FIG. 6. *Histogram showing the energy distribution of γ-rays of neutron capture in sodium. Dotted line shows the full spectrum obtained; solid line is the final result after subtraction of background. The peak at 2.8 Mev. is presumed to be the 2.76 Mev. γ-ray accompanying the β-decay of* Na^{24}.

Fig. 6 is a histogram of the γ-rays of neutron capture in Na^{23}. A feature of this spectrum is the narrow peak at 2.8 Mev., presumably from the 2.76 Mev. γ-ray accompanying the β-decay of Na^{24} which is produced in this experiment.

TABLE II

COMPARISON OF OBSERVED PEAKS IN CAPTURE γ-RAY SPECTRUM OF SODIUM WITH POSSIBLE OBSERVABLE γ-RAYS CALCULATED FROM ENERGY LEVEL SCHEME OF Na^{24}

Calculated γ-ray energies, Mev.	Observed γ-ray peaks, Mev.	Observed relative intensities
2.76*	2.7_9*	45
2.97	—	—
3.00	3.0_5	61
3.38	3.2_5	56
—	3.5_5	70
—	3.9_2	39
—	4.3_5	89
—	4.8_2	100
5.09	5.3_7	31
5.97	—	—
6.35	—	—

* *γ-ray of* Mg^{24}.

From this peak the resolving power of the method at its lower energy limit was estimated. Examination of this spectrum indicates that it consists of several lines, and Fig. 7 shows an attempt to fit the observed points by means of a series of eight Gaussians of half-widths as determined from Fig. 3. Murrell and Smith (12) have shown that Na^{24} has energy levels at 0.38, 1.26, and 3.38

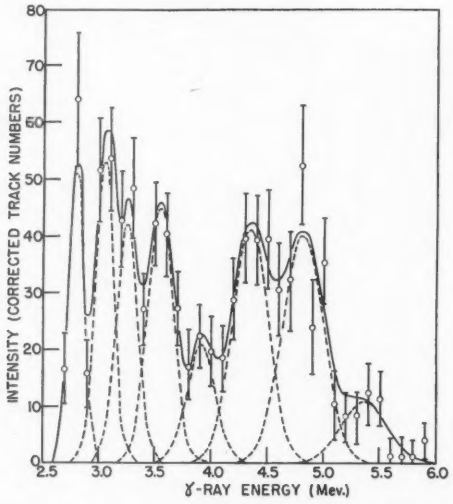

FIG. 7. *Observed spectrum of γ-rays of neutron capture in sodium fitted with a composite curve consisting of eight Gaussians (shown dotted) of energy and intensity as given in Table II, and of half-widths as determined from Fig. 3. Limits shown on individual points are standard deviations.*

Mev., and the excitation from the mass excess of the captured neutron is 6.35 Mev. Table II compares the possible γ-rays from decay via these levels with the γ-ray energies and intensities used in fitting the composite curve to the histogram.

III. γ-Rays Following the Decay of N^{16}

The effluent cooling water of the Chalk River pile contains a source of high energy γ-rays. By measuring the γ-ray activity at points along the discharge pipe in which the flow rate is known, the half life of the activity was measured as 7.3 sec. Since the half life of N^{16}–a known high energy γ-ray emitter–is 7.35 sec. (2), it was deduced that the activity was due to N^{16} produced by the reaction $O^{16}(n, p)N^{16}$ in the cooling water as it passed through the pile.

A lead collimator, 3 in. in thickness, was constructed facing the effluent water pipe, and a deuterium-loaded plate placed inside it so that γ-rays from the pipe entered the plate within 20° of the normal to the surface of the emulsion. The plate was left in this position until maximum tolerable γ-ray fogging had been obtained. To estimate background, a second deuterium-loaded plate

was exposed in an equivalent position, but shielded from γ-rays by approximately one foot of lead.

The plates were searched, tracks measured, and γ-ray spectra calculated by the method previously described. Fig. 8 shows the background spectrum, and Fig. 9 the spectrum found on the plate exposed to N^{16} γ-rays.

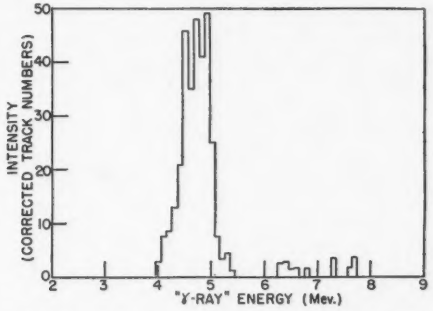

FIG. 8. *Histogram showing background spectrum for the study of the γ-rays following the β-decay of N^{16}.*

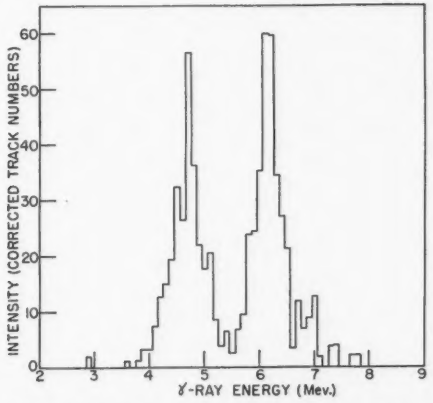

FIG. 9. *Histogram showing the energy distribution of the γ-rays following the β-decay of N^{16}. Background has not been subtracted.*

The background is mainly due to α-particle tracks from naturally radioactive contaminants in the emulsion, and is, fortunately, negligible in the region of 6 to 7 Mev. The N^{16} spectrum in this region consists of a single peak with a shoulder on the high energy side which indicates a secondary peak in the 7 Mev. region. Preliminary measurements indicated that the main peak corresponded to a γ-ray energy of about 6.2 Mev., and this was therefore identified as being from the decay of N^{16} via the 6.124 Mev. (4) level of O^{16}. From this identifi-

cation the correct range–energy relationship for the emulsion was determined as described in Section II and the corrected histograms plotted.

It is known that there are two O^{16} energy levels in the 7 Mev. region which might account for the high energy γ-rays from N^{16}, the latest measurement of their values being 6.897 and 7.099 Mev. (4). Inspection of the histogram indicates that most, if not all, of the high component corresponds to decay via the lower of these two levels. We have therefore assigned tentatively an energy of 6.897 Mev. to the subsidiary peak.

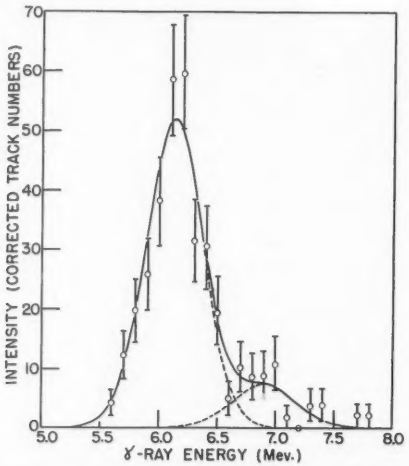

FIG. 10. *Observed spectrum of γ-rays following the decay of N^{16} fitted with a composite curve consisting of two Gaussians of energies 6.124 and 6.897 Mev. and relative intensities of 7: 1. Half-width of the main peak was found to be 0.565 Mev.; the half-width of the secondary peak was assumed to be 0.633 Mev.*

In order to estimate the relative intensities of the two γ-ray lines, a Gaussian curve was fitted to the main peak, a second curve of appropriate half-width was drawn at 6.897 Mev., and the resultant composite curve compared with the observed data. Fig. 10 shows the fitting obtained in which the relative heights of the two peaks are as 7 to 1. We have shown by application of the χ^2 test that the fit of this composite curve is satisfactory (8, pp. 186-191).

IV. Conclusions

Energies and relative intensities of high energy γ-rays may be studied by means of Ilford type C2 emulsions loaded with hexadeutero diacetin and exposed to one or two roentgens of the radiation. The method is most effective from about 3 to 6 Mev. over which region the resolving power (i.e., width at half-maximum of a single line) varies with energy from approximately 0.2 to 0.6 Mev. The method is, however, inferior in range, accuracy, resolving power,

and speed to the pair spectrometric method (17) and should be considered only if a pair spectrometer is not available, or if γ-ray intensities are low.

The spectrum of γ-rays of neutron capture in cadmium appears in general to be an unresolved spectrum decreasing with energy up to about 7.5 Mev. The capture γ-ray spectra of sodium and chlorine, on the other hand, show a number of distinct lines, some of which can be correlated with transitions between known energy levels of the excited nuclei.

The γ-ray emitting modes of decay of N^{16} are found to be via the 6.124 and probably the 6.897 Mev. levels of O^{16} with relative intensities of 7:1 respectively.

Acknowledgments

We should like to thank Dr. B. W. Sargent for his interest and advice on these experiments, and Mr. R. G. Hayman for his assistance in searching and measuring some of the plates. We are also indebted to Dr. A. Morrison of the National Research Laboratories, Ottawa, for making the deuterium-loaded plates available to us, and to Dr. E. P. Blizard of the Oak Ridge National Laboratory for suggesting to us the measurement of the N^{16} γ-rays.

References

1. Bell, R. E. and Elliott, L. G. Phys. Rev. 74: 1552. 1948.
2. Bleuler, E., Scherrer, P., Walter, M., and Zünti, W. Helv. Phys. Acta, 20: 96. 1947.
3. Coltman, J. W. and Goldhaber, M. Phys. Rev. 69: 411. 1946.
4. Fowler, W. A. Private communication.
5. Gibson, W. M., Green, L. L., and Livesey, D. L. Nature, 160: 534. 1947.
6. Goldhaber, G. Phys. Rev. 74: 1725. 1948.
7. Hamermesh, B. Phys. Rev. 76: 182. 1949.
8. Hoel, P. G. Introduction to mathematical statistics. John Wiley & Sons, Inc., New York. 1947.
9. Lattes, C. M. G., Fowler, P. H., and Cuer, P. Proc. Phys. Soc. (London), 59: 885. 1947.
10. Margenau, H. and Murphy, G. M. The mathematics of physics and chemistry. D. Van Nostrand Company, Inc., New York. 1943.
11. Moak, C. D. and Dabbs, J. W. T. Phys. Rev. 75: 1770. 1949.
12. Murrell, E. B. M. and Smith, C. L. Proc. Roy. Soc. (London), A, 173: 410. 1939.
13. Overman, R. T. Radioactivities produced in the neutron irradiation of chlorine. AECD-857. 1947.
14. Pais, A. Kgl. Danske Videnskab. Selskab, Mat.-fys. Medd. 20(17): 4. 1943.
15. Rosenfeld, L. Nuclear forces I. Interscience Publishers, Inc., New York. 1948
16. Shrader, E. F. and Pollard, E. Phys. Rev. 59: 277. 1941.
17. Walker, R. L. and McDaniel, B. D. Phys. Rev. 74: 315. 1948.

TWO NEW $^2\Sigma - {}^2\Sigma$ SYSTEMS DUE TO THE MOLECULE NO[1]

By M. W. Feast

Abstract

The emission band system at 6000Å found in discharges in flowing NO_2 and attributed to NO^+ by Jausserant, Grillet, and Duffieux has been examined at high dispersion and shown to be due to the transition of $E^2\Sigma^+$ (a new level) $\rightarrow$ $A^2\Sigma^+$ (the upper state of the γ system) of the NO molecule. The rotational and vibrational analysis of the system is given. The band system corresponding to the transition $D^2\Sigma^+$ (upper state of the ϵ system of NO) $\rightarrow A^2\Sigma^+$ at 11,000 Å has also been observed and its analysis is presented. The separate nature of the $D^2\Sigma^+$ state from the $A^2\Sigma^+$ state is thus supported. Some brief remarks on other band structures found in discharges in flowing NO_2 are included.

I. Introduction

Some years ago Jausserant, Grillet, and Duffieux (2, 3, 11) reported the occurrence of a headless band near 6000Å in emission from a low pressure discharge in flowing NO_2 or NO. These writers concluded that the band consisted of three close *P* branches and three close *R* branches and that it therefore corresponded to a transition between triplet states. Since the NO molecule can give rise only to states of even multiplicity it was concluded that the band was emitted by the molecule NO^+ (which of course would give only odd multiplicity states). In the present paper it is shown that the band structure is in fact due to NO, and another headless band at about 11,000Å occurring under the same experimental conditions as the 6000Å band is also shown to be due to NO.

II. Experimental Arrangements and Appearance of Spectra

The discharge tube used in this investigation was a normal type of water cooled positive column "end-on" tube with electrodes of tantalum in the form of hollow cylinders. A rapid stream of NO_2 from a cylinder of compressed gas was passed through the tube and the discharge was activated by a 6000 v.2kva. transformer. The rate of flow of NO_2 was such that band spectra of N_2 formed by decomposition of the NO_2 were weak or absent. Under these conditions the discharge was purple in color and concentrated towards the axis of the tube. Close to the walls of the discharge tube there was a green glow which gave a continuous spectrum probably identical with the well known air afterglow continuum. The spectrum was photographed between 2000Å and 13,000Å at low dispersion (Hilger E.2 with glass and quartz optics), between 3600Å and 11,200Å in the first order of an Eagle mounting 21 ft. grating spectrograph (15,000 lines/in.), and in the region 6000Å in the second order of this grating. The band structure near 6000Å required exposure times of about five minutes in the first order and five hours in the second order (with Kodak 103*a*F plates)

[1] *Manuscript received April 13, 1950.*
Contribution from the Division of Physics, National Research Laboratories, Ottawa, Canada. Issued as N.R.C. No. 2182.

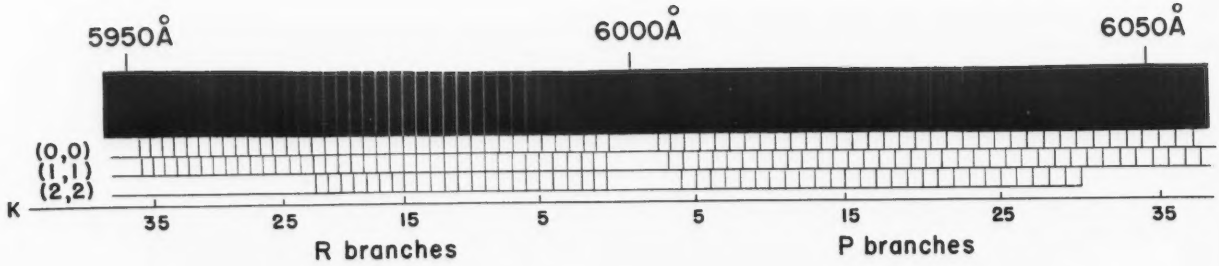
5950Å
6000Å
6050Å
(0,0)
(1,1)
(2,2)
K
35
25
15
5
5
15
25
35
R branches
P branches

whilst the structure at 11,000Å required an exposure of 33 hr. in the first order (with hypersensitized Kodak I-Z plates).

In the ultraviolet region the discharge shows bands due to the well known NO γ system. Bands of the NO ϵ and δ systems also occur. The headless band at 6000Å is the strongest emission in the visible region. The high dispersion spectrograms also show that there is a very complex spectrum extending throughout most of the visible region. There is little regularity apparent in this structure but there are two fairly sharp maxima of intensity near 5400Å and a broad maximum near 5500Å. At low dispersion the spectrum in this region is very similar to the one observed by Schüler and Woeldike (13) from low current discharges in NO_2. It seems likely that these bands are due to some polyatomic combination of nitrogen and oxygen (NO_2 ?). At about 7800Å and 8600Å small dispersion spectrograms show groups of band heads which bear considerable resemblance to the first negative O_2^+ bands ($^4\Sigma \rightarrow {}^4\Pi$). Bearing in mind that O_2^+ and NO are isoelectronic it seems possible that these bands represent the analogous NO transition. In the further infrared there are bands at 9680Å and 10370Å, the latter being too weak for a high dispersion investigation of its structure. The structure of the 9680Å band is relatively simple and it is probably a $\Pi \rightarrow \Sigma$ transition; it is hoped to investigate this band in more detail at a later date. Finally, band structure has been found near 11,000Å, whose analysis will be presented in this paper, whilst small dispersion spectrograms reveal a band in the region near 13,000Å which could not be photographed at high dispersion.

III. Analysis of the 6000Å Band System

Previous work on this band structure has been outlined above and it has been noted that the triplet structure of the branches led to the identification of the emitter as NO^+. However, though formulas were given by Jausserant, Grillet, and Duffieux (11) for the wave numbers of the lines in each band, no rotational analysis was made and the actual wave numbers of the lines were not tabulated. The present work shows that the band structure does indeed consist of three R and three P branches but it will be clear from the plate that it is not possible to consider these branches as due to a spin tripling of the electronic levels involved in the emission. On the other hand for headless bands where $B' \cong B''$ it is known that the origins of bands in any one sequence will lie very close together, and hence it is possible to attempt an analysis of the band structure on the assumption that it consists of three overlapping bands each with a single P and R branch. From a consideration of the Franck–Condon principle in cases where $B' \cong B''$, $\omega' \cong \omega''$ it is natural to take the bands as the (0, 0), (1, 1), and (2, 2) bands of the system.

The wave numbers of the band lines are given in Table I together with their analysis. They were obtained from the spectra taken in the second order of the 21 ft. grating (1.34 Å/mm. at 6000Å). The spectra were measured against iron arc lines, the wave lengths of the latter being taken from the M.I.T. Wavelength Tables, and the conversion into wave numbers being made using

Kayser's "Tabelle der Schwingungzahlen". The wave numbers should be accurate to ± 0.02 cm.$^{-1}$. As can be seen from Table I the three R branches are blended together over a considerable range. In determining the molecular constants, only unblended lines have been used. It will be noted that it has not been found possible to measure a few of the lines close to the origin. For instance in the (0, 0) band, three lines are missing when the P and R branches are arranged in a single series. Obviously one of these is the true missing line (band origin) and the others correspond to very weak though permissible lines. Thus it is conceivable that any one of these three lines might be the true missing line

TABLE I

WAVE NUMBERS AND ANALYSIS OF 6000Å SYSTEM

K	(0, 0) Band		(1, 1) Band		(2, 2) Band	
	R branch	P branch	R branch	P branch	R branch	P branch
1	16671.47		16672.02		16672.02	
2	675.41	16655.69	675.94		675.94	
3	679.33	651.67	679.72	16652.33	679.72	
4	683.19	647.63	683.60	648.25	683.60	16648.69
5	687.07	643.60	687.44	644.31	687.44	644.86
6	690.88	639.52	691.24	640.31	691.24	640.85
7	694.78	635.47	695.01	636.27	695.01	636.84
8	698.71	631.41	698.71	632.22	698.71	632.87
9	702.49	627.26	702.49	628.16	702.49	628.81
10	706.23	623.16	706.23	624.09	706.23	624.77
11	709.98	619.04	709.98	620.01	709.98	620.71
12	713.72	614.88	713.72	615.91	713.72	616.66
13	717.40	610.72	717.40	611.81	717.40	612.59
14	721.12	606.55	721.12	607.64	721.12	608.52
15	724.80	602.37	724.80	603.51	724.54	604.40
16	728.46	598.16	728.46	599.34	728.16	600.27
17	732.10	593.94	732.10	595.18	731.72	596.13
18	735.72	589.71	735.72	590.97	735.30	592.02
19	739.32	585.47	739.32	586.80	738.86	587.82
20	742.88	581.21	742.88	582.56	742.39	583.68
21	746.44	576.91	746.44	578.32	745.88	579.47
22	750.09	572.62	749.89	574.07	749.43	575.26
23	753.60	568.34	753.39	569.81	752.90	
24	757.14	564.00	756.87	565.54	756.35	566.89
25	760.64	559.68	760.32	561.22	759.78	562.61
26	764.10	555.33	763.73	556.94	763.15	558.35
27	767.57	550.95	767.19	552.64	766.66	554.04
28	771.01	546.62	770.60	548.27	769.97	549.83
29	774.41	542.23	773.97	543.96		545.57
30	777.82	537.82	777.38	539.66		
31	781.18	533.37	780.72	535.27		
32	784.52	528.96	784.05	530.90		
33	787.84	524.48	787.29	526.52		
34	791.18	520.03	790.67	522.11		
35	794.49	515.59	793.86	517.73		
36	797.83	511.14	797.07	513.27		
37		506.67		508.96		

Note on Table I:

The intensity distribution in the bands is normal except that $P_{2,2}(14)$ is abnormally weakened. Since neither $R_{2,2}(14)$ nor $R_{2,2}(12)$ are resolved it is impossible to decide whether this is an effect in $E^2\Sigma$ or $A^2\Sigma$; however, since nothing of this kind has apparently been observed in the γ bands it is natural to attribute it to some abnormality in the $E^2\Sigma$ state. The exact cause of this is not clear.

and the K numbering is not unambiguously defined. However, the symmetrical intensity distribution in the two branches makes the center one of these lines the obvious choice of the origin. The K numbering thus obtained is accepted here and is very strongly supported by the identification of the lower state of the system with a previously known state of NO as described below. The other two bands were treated in a similar manner. From Table I the combination

TABLE II

K	$\Delta_2''(F)$ 6000Å system $v'' = 1$	$\Delta_2'(F)$ 1, 0 γband $A^2\Sigma - X^2\Pi_{1/2}$	$\Delta_2'(F)$ 1, 0 γband $A^2\Sigma - X^2\Pi_{3/2}$
2	19.69	19.91?	19.27?
3	27.69	27.58?	27.62?
4	35.41	35.34?	35.26?
5	43.29	43.27?	43.18?
6	51.17	51.51?	51.20?
7	59.02	59.27?	58.98
8	66.85	67.13?	67.09
9	74.62?	74.44?	75.06
10	82.48?	82.76?	82.59
11	90.32?	90.67?	90.46
12	98.17?	98.52?	98.29
13	106.08?	106.29?	106.46
14	113.89?	114.07?	113.98
15	121.78?	121.96?	121.94
16	129.62?	129.69?	129.33
17	137.49?	137.67?	137.39
18	148.30?	145.56	145.63
19	153.16?	153.25	153.13
20	161.00?	160.95	160.91
21	168.81?	168.82	168.41
22	176.63	176.58	176.49
23	184.35	184.51	184.46
24	192.17	192.37	192.26
25	199.93	199.98	200.19
26	207.68	208.01	207.89
27	215.46	215.69	215.36
28	223.23	223.37	223.33
29	230.94	321.02	231.01
30	238.70	238.92	238.90
31	246.48	246.55	246.68
32	254.20	254.35	254.23
33	261.94	261.90	262.36
34	269.56	269.63	269.72
35	277.40	277.59	277.57
36	284.90	284.84	284.91

Note on Table II:

Differences marked (?) are obtained from two lines one at least of which is a blend. This affects the accuracy slightly.

differences $\Delta'_2F(K) = R(K) - P(K)$ and $\Delta''_2F(K) = R(K-1) - P(K+1)$ are easily computed. To save space all these differences are omitted except those for the state $v'' = 1$, which are given in the first column of Table II.

Since each band consists of a single P and R branch it would appear that the transition is $^1\Sigma \rightarrow {}^1\Sigma$. However, comparison of the combination differences

of the lower state of this band system with those of the upper state of the NO γ band system ($A^2\Sigma^+$) shows that these two states are the same. Combination differences for the $A^2\Sigma^+$ state of NO for $v = 0, 1, 2$ (actually $\Delta_1F(K)$ values from which the $\Delta_2F(K)$ values are easily derived) are tabulated by Schmid, Konig, and Farkas (12), and these were found to agree with the values of the combination differences for the three lower vibrational levels of the 6000Å system, within the experimental error. For the level $v = 1$ it is possible to obtain combination differences for the $A^2\Sigma^+$ state from the measurements of Gerö and Schmid (7) which are of considerably greater accuracy than those given by Schmid, Konig, and Farkas. The two sets of $\Delta_2F(K)$ values obtained from the two sub-bands of the (1, 0) γ band as measured by Gerö and Schmid are tabulated in Table II. It will be seen that the combination differences obtained from the 6000Å band agree with the two sets of $A^2\Sigma^+$ state differences as well as the latter agree with each other. The transition for the system is therefore $^2\Sigma^+ \rightarrow A^2\Sigma^+$ (since $\Sigma^- \rightarrow \Sigma^+$ is forbidden). The upper state has not been found before and will be designated $E^2\Sigma^+$. The fact that no doublet splitting is observed in the bands of this system is in agreement with the fact that such a splitting has not yet been detected in any of the NO $^2\Sigma$ states.

In determining the rotational constants B and D for the various vibrational levels the formula $\dfrac{\Delta_2F(K)}{4K+2} = B + 2D(K + \frac{1}{2})^2$ was assumed to hold and the constants were determined graphically from a plot of $\Delta_2F(K)/4K + 2$ against $(K + \frac{1}{2})^2$. The values of these constants and others derived from them are given in Table III in which all the symbols have their usual significance. Using the values of B_v the constants B_e and α were determined as the best values for the formula $B_v = B_e - \alpha(v + \frac{1}{2})$.

TABLE III

ROTATIONAL CONSTANTS FROM 6000Å BAND SYSTEM

Lower state, $A^2\Sigma^+$	Upper state, $E^2\Sigma^+$
$B_e'' = 1.9948 \pm 0.001$ cm.$^{-1}$ $B_0'' = 1.9856$ cm.$^{-1}$ $B_1'' = 1.9679$ cm.$^{-1}$ $B_2'' = 1.9488$ cm.$^{-1}$ } ± 0.0005 cm.$^{-1}$ $\alpha'' = 0.0184 \pm 0.001$ cm.$^{-1}$	$B_e' = 1.9863 \pm 0.001$ cm.$^{-1}$ $B_0' = 1.9772$ cm.$^{-1}$ $B_1' = 1.9591$ cm.$^{-1}$ $B_2' = 1.9408$ cm.$^{-1}$ } ± 0.0005 cm.$^{-1}$ $\alpha' = 0.0182 \pm 0.001$ cm.$^{-1}$
$D_0'' = 5.3 \times 10^{-6}$ cm.$^{-1}$ $D_1'' = 6.0 \times 10^{-6}$ cm.$^{-1}$ $D_2'' = 5.9 \times 10^{-6}$ cm.$^{-1}$ $D_e'' = 5.6 \times 10^{-6}$ cm.$^{-1}$ } $\pm 0.2 \times 10^{-6}$ cm.$^{-1}$	$D_0' = 5.2 \times 10^{-6}$ cm.$^{-1}$ $D_1' = 5.6 \times 10^{-6}$ cm.$^{-1}$ $D_2' = 5.9 \times 10^{-6}$ cm.$^{-1}$ $D_e' = 5.6 \times 10^{-6}$ cm.$^{-1}$ } $\pm 0.2 \times 10^{-6}$ cm.$^{-1}$
$r_e'' = 1.0637$ (± 0.0001) $\times 10^{-8}$ cm. $\beta'' = 2 \times 10^{-8}$ cm.$^{-1}$ (approx.)	$r_e' = 1.0660$ (± 0.0001) $\times 10^{-8}$ cm. $\beta' = 2 \times 10^{-8}$ cm.$^{-1}$ (approx.)

The accuracy of the D_v values is not great enough for D_e to be determined from these alone but assuming the value of β in the formula $D_v = D_e + \beta(v + \frac{1}{2})$ as given by

$$\beta = -\frac{a^2}{6\omega_e} + D_e\left(\frac{8\omega_e x_e}{\omega_e} - \frac{5a}{B_e}\right) \qquad \text{(Herzberg (9))}$$

a rough value for D_e can be obtained. Within the experimental error this agrees with the D_e values given in Table III which were obtained from the formula $D_e = \frac{4B_e^3}{\omega_e^2}$. r_e was determined from the formula $r_e = \sqrt{\frac{h}{8\pi^2\mu B_e}}$ using the Atomic Constants of DuMond and Cohen (4). The formula with these constants reduces to: $r_e = \frac{4.10610}{\sqrt{\mu_A B_e}} \cdot 10^{-8}$ cm., where μ_A = reduced mass of NO ($O^{16} = 16$). Of the previous determinations of the constants of the $A^2\Sigma$ state the most accurate are those of Gerö and Schmid (7). Their values of B differ from the present ones by more than 0.001 cm.$^{-1}$ only in the case of $v = 0$ (differences of the order 0.001 cm.$^{-1}$ are to be expected if the probable error in both cases is of the order 0.0005 cm.$^{-1}$). The difference in the B values for $v = 0$ (= 0.0014 cm.$^{-1}$) can be traced to a difference in the methods of determining this constant. In Gerö and Schmid's method, D is assumed to be 6.0×10^{-6} cm.$^{-1}$ for all levels and B is determined on this assumption. Using this method on the present data, the two sets of B values are found to agree to well within the experimental error.

The determination of the band origins was also carried out graphically using the formula $R(K-1) + P(K) = 2\nu_0 + 2(B' - B'')K^2$. By plotting $R(K-1) + P(K) - 2(B' - B'')K^2$ against K^2, ν_0 is obtained and the value of $B' - B''$ is

TABLE IV

VIBRATIONAL CONSTANTS FOR THE 6000Å BAND SYSTEM

ν_e = 1662.87 cm.$^{-1}$ (The accuracy depends on the unknown accuracy of ω_e'' and $x_e''\omega_e''$)
$\nu_{0,0}$ = 16663.63 cm.$^{-1}$
$\nu_{1,1}$ = 16664.15 cm.$^{-1}$ } Relative accuracy probably ± 0.02 cm.$^{-1}$
$\nu_{2,2}$ = 16664.43 cm.$^{-1}$

$A^2\Sigma^+$ state ω_e'' = 2371.3 cm.$^{-1}$ $\quad x_e''\omega_e''$ = 14.48 cm.$^{-1}$ (see (7))
$E^2\Sigma^+$ state ω_e' = 2373.66 cm.$^{-1}$ $\quad x_e'\omega_e'$ = 15.87 cm.$^{-1}$

checked. The band origins, the system origin, and the vibrational constants in the upper and lower states are listed in Table IV. It is clearly not possible to separate out the two sets of vibrational constants from a single sequence of bands. Therefore the values of these constants for the $A^2\Sigma$ state are taken from the work of Gerö and Schmid (7) and the constants for the $E^2\Sigma$ state derived by combining these with the ν_0 values. It may be mentioned here that no trace could be found of the (1, 0) or (0, 1) sequences; they would of course be expected to be very weak from a consideration of the Franck–Condon principle. The relation of the $E^2\Sigma$ level to the other NO energy levels is shown in the figure.

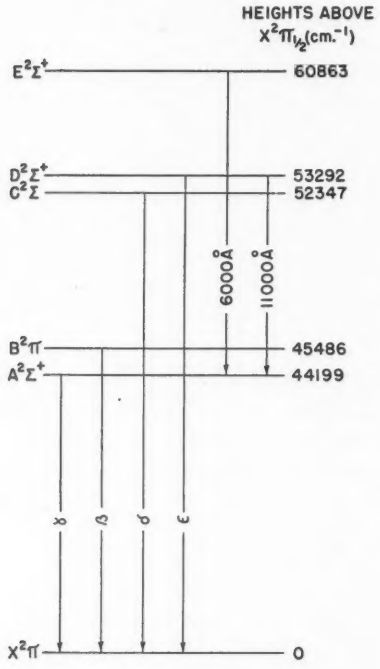

IV. Analysis of the 11,000Å Band System

It will be clear from the energy level diagram that there is a possibility of observing the following further $^2\Sigma - {}^2\Sigma$ transitions of NO: — $E^2\Sigma \rightarrow D^2\Sigma$ ($\backsim$13212Å); $E^2\Sigma \rightarrow C^2\Sigma$ ($\backsim$11743Å); $D^2\Sigma \rightarrow A^2\Sigma$ ($\backsim$11,000Å); $C^2\Sigma \rightarrow A^2\Sigma$ ($\backsim$12273Å). All these states have potential curves and equilibrium internuclear distances very similar to the $A^2\Sigma$ state, and hence all the above band systems would be expected to be similar in appearance to the 6000Å system. However, the transitions involving the $C^2\Sigma$ state are possible only if this is $^2\Sigma^+$, and it is not known whether this is so or not. The fact that no bands are observed at 11743Å or 12273Å suggests that the C state is $^2\Sigma^-$ but there may of course be other reasons for these systems being weak or missing. Observation of bands involving the $D^2\Sigma$ state is of considerable interest since the actual existence of this state has been in doubt for some time. The $D^2\Sigma$ state is the upper state of NO ϵ bands but Herzberg and Mundie (10) concluded that these bands were actually part of the NO γ system, and the levels previously denoted by $D^2\Sigma$, $v = 0, 1, 2$ were in fact $A^2\Sigma$, $v = 4, 5, 6$. On the other hand Gaydon (5, 6) and Gerö, Schmid, and Szily (8) examined the rotational and vibrational structure of the NO ϵ bands in detail. They found that if these bands were treated as part of the NO γ system there would be sharp discontinuities in all the mole-

cular constants at $A^2\Sigma$, $v = 4$ (i.e., $D^2\Sigma$, $v = 0$). They concluded that this was not permissible and therefore considered the existence of the $D^2\Sigma$ state to be established. However, this did not entirely rule out the possibility of some large perturbation taking place at $A^2\Sigma$, $v = 4$. It is shown below that the band structure observed at 11,000Å is due to the transition $D^2\Sigma \rightarrow A^2\Sigma$. It does not seem very likely that this relatively strong and isolated band system could be a rotational–vibrational transition in the $A^2\Sigma$ state as would be required by Herzberg and Mundie's interpretation of the NO ϵ bands, and hence the present work supports the conclusion that the $D^2\Sigma$ state has a separate existence. Whilst this seems the most straightforward interpretation of the spectrum, Dr. Herzberg has pointed out to the author that this leads to difficulties in the interpretation of the absorption spectrum of NO, since Professor Tanaka (private communication to Dr. Herzberg) finds no bands of the NO γ system in absorption with $v' > 3$ (assuming the ϵ bands as a separate system) whereas there is every reason to believe they should occur. Under the conditions of the large perturbations envisaged by the Herzberg–Mundie interpretation, it is possible that a rotational–vibrational transition might have the required intensity. It is hoped to investigate the spectrum of $N^{15}O$ and hence settle this point conclusively by means of the isotope effect. To avoid confusion in the discussion of the analysis of the 11,000Å band system the $D^2\Sigma$ state is considered as a separate state.

The 11,000Å band was photograped in the first order of the 21 ft. grating (2.64Å/mm. at 11,000Å) and measured against iron arc lines in the overlapping third order, since there are no accepted wave length standards in the 11,000Å region. In a subsidiary experiment it was shown that near 9000Å the coincidence error of the grating was less than 0.02Å (measured in the first order). The wave lengths of the iron lines were taken from the M.I.T. Wave-length Tables, tripled and corrected to vacuum, using the refractive indices of air as determined by Barrell and Sears (1).

At high dispersion the band system appears to consist simply of a single headless band (one P and one R branch) with two other bands to slightly longer wave lengths. The two latter bands are weaker than the first band and their lines are somewhat blended with each other and also with the lines of the strong band. Analysis of the strong band shows it to be the (0, 0) $D^2\Sigma^+ \rightarrow A^2\Sigma^+$ band. A determination of the combination differences for the other two bands shows them to be (1, 1) and (2, 2) bands of the system. However, owing to the meagerness of the data on these bands it has been decided to give data on the (0, 0) band only. The wave numbers and analysis of this band are given in Table V. The wave numbers should be accurate to ± 0.02 cm.$^{-1}$. The K numbering, combination differences, and rotational constants for the band were determined in a manner similar to that described for the 6000Å band system. The values of $\Delta_2''(F)$ and $\Delta_2'(F)$ agree well with the values for the $A^2\Sigma$ state given in Table II and for the $D^2\Sigma$ state calculated from the work of Gerö, Schmid, and Szily (8). There are however some minor differences due in part to the

experimental error and also due to the fact that many of the lines of the 11,000Å (0, 0) band are blended with lines of the (1, 1) and (2, 2) bands. For this reason the constants determined for the $A^2\Sigma$ state from this band are not considered as accurate as those determined from the 6000Å band, and no

TABLE V

ANALYSIS OF THE (0, 0) BAND, $D^2\Sigma^+ \rightarrow A^2\Sigma^+$ SYSTEM

K	$R(K)$	$P(K)$	K	$R(K)$	$P(K)$
2		9085.10	17	9165.03	9025.97
3	9108.04	9080.57	18	9169.19	9022.17
4	9112.16	9076.33	19	9173.32	9018.25
5	9116.21	9072.38	20	9177.43	9014.62
6	9120.19	9068.43	21	9181.62	9010.84
7	9124.26	9064.60	22	9185.75	9007.08
8	9128.27	9060.64	23	9189.89	9003.34
9	9132.39	9056.77	24	9194.05	8999.54
10	9136.42	9052.87	25	9198.10	8995.83
11	9140.53	9048.97	26	9202.35	8992.10
12	9144.63	9045.13	27	9206.53	8988.43
13	9148.64	9041.28	28		8984.72
14	9152.75	9037.42	29		8981.01
15	9156.89	9033.61	30		8977.35
16	9160.98	9029.76	31		8973.98
			32		8970.10

attempt was made to average the two determinations. The value of B_0'' came out to 1.9866 cm.$^{-1}$ (from the 6000Å system $B_0'' = 1.9856$ cm.$^{-1}$) the agreement therefore being satisfactory. D_0'' is not significantly different from the value given in Table III. For the $D^2\Sigma$ state the rotational constants also agree well with those given by Gerö, Schmid, and Szily:—

Gerö, Schmid and Szily $B_0' = 1.9917$ cm.$^{-1}$ $D_0' = 6.1 \times 10^{-6}$ cm.$^{-1}$

11,000Å system $B_0' = 1.9912$ cm.$^{-1}$ $D_0' = 5.8 \times 10^{-6}$ cm.$^{-1}$

The origin of the (0, 0) 11,000Å band was determined as $\nu_0 = 9092.17$ cm.$^{-1}$ with a probable error of about 0.05 cm.$^{-1}$. Gerö, Schmid, and Szily give the $D^2\Sigma$ ($v = 0$ $K = 0$) level as 53291.9 cm.$^{-1}$ above the ground state, and Gerö and Schmid (7) give the height of the $A^2\Sigma$ ($v = 0$ $K = 0$) level as 44199.2 cm.$^{-1}$. This gives the origin of the $D^2\Sigma \rightarrow A^2\Sigma$ system as 9092.7 cm.$^{-1}$. It is difficult to assess the probable error of this value but since it is the difference of two quantities whose individual errors might perhaps be as great as 0.2 to 0.4 cm.$^{-1}$ it does not differ significantly from the more accurate value determined from the 11,000Å system.

In conclusion it may be stated that the band observed under small dispersion in the 13,000Å region may quite probably be $E^2\Sigma \rightarrow D^2\Sigma$.

Acknowledgments

The author wishes to acknowledge the helpful discussions he has had with Dr. G. Herzberg in the course of this work. He has also benefitted from discussions with Dr. A. E. Douglas on the various problems that have arisen.

References

1. BARRELL, H. and SEARS, J. E. Phil. Trans. Roy. Soc. A, 238: 1. 1939.
2. DUFFIEUX, M. and GRILLET, L. Compt. rend. acad. sci. Paris, 201: 1338. 1935.
3. DUFFIEUX, M. and GRILLET, L. Compt. rend. acad. sci. Paris, 202: 938. 1936.
4. DUMOND, J. W. M. and COHEN, E. R. Revs. Modern Phys. 20: 82. 1948.
5. GAYDON, A. G. Proc. Phys. Soc. (London), 56: 95. 1944.
6. GAYDON, A. G. Proc. Phys. Soc. (London), 56: 160. 1944.
7. GERÖ, L. and SCHMID, R. Proc. Phys. Soc. (London), 60: 533. 1948.
8. GERÖ, L., SCHMID, R., and SZILY, F. K. VON. Physica, 11: 144. 1944.
9. HERZBERG, G. Molecular spectra and molecular structure, Vol. 1, p. 116. 1st ed. Prentice-Hall, Inc., New York. 1939.
10. HERZBERG, G. and MUNDIE, L. G. J. Chem. Phys. 8: 263. 1940.
11. JAUSSERANT, C., GRILLET, L., and DUFFIEUX, M. Compt. rend. acad. sci. Paris, 205: 39. 1937.
12. SCHMID., R., KONIG, T., and FARKAS, VON D. Z. Physik., 64: 84. 1930.
13. SCHÜLER, H. and WOELDIKE, A. Physik. Z. 45: 171. 1944.

ENERGY DISTRIBUTION OF FISSION FRAGMENTS FROM Pu^{239}[1]

By D. C. Brunton and W. B. Thompson[2]

Abstract

The measurement of the energy distribution of fission fragments has been extended to include fragments from fission in Pu^{239}. The same equipment was used as in previous experiments on U^{235} and U^{233}. The experimental results parallel very closely those obtained in the previous work. The values obtained for the most probable energies for the light and heavy fragments from Pu^{239} are 94.6 and 65.2 Mev. respectively. The statistical accuracy of the data is, as before, an improvement over earlier work in this field, and a more detailed comparison of the three materials is made possible.

I. Introduction

For the purpose of comparing different nuclides fissile by slow neutrons the measurements of the energy distribution of fission fragments have been extended to the nuclide Pu^{239}. The experimental arrangement and the detailed results for the nuclides U^{235} and U^{233} have been reported previously (1, 2). A note briefly describing the experimental results for Pu^{239} has already been published (3).

The energy distribution of the fission fragments from Pu^{239} had been measured earlier by Deutsch and Ramsey (5), but it was felt worth while to repeat this work, since higher statistical accuracy could be readily obtained with the equipment of Brunton and Hanna (2).

II. Experimental Conditions

The double "back-to-back" ionization chamber and the electronic equipment, including the 30-channel pulse analyzer, were the same as previously described (2). The fission source and the neutron source were slightly different.

As before, the fission source was prepared by dissolving a fissile material (in this case a plutonium compound) in amyl acetate, which was used as the solvent in the preparation of a collodion film by evaporation on a water surface. Plutonium nitrate was chosen, and owing to the solubility of this compound in water a fast drying film solution was used (35% collodion (93 mgm. per ml.), 65% amyl acetate). Thus, the time in contact with water was reduced to a few seconds. After removal from the surface of the water the film was allowed to dry nearly completely before being laid on the collimator. In this way, practically no water was available for the formation of fillets in the collimator holes and a more nearly perfect source obtained. The figure of merit, R, used for these sources (2) is the ratio of counts in the collimated chamber to true coincidence counts, and for this plutonium source $R = 1.05$. To maintain adhesion of the

[1] *Manuscript received May 11, 1950.*
Contribution from the Nuclear Physics Branch, Division of Atomic Energy Research, National Research Council of Canada, Chalk River, Ontario. Issued as N.R.C. No. 2186.
[2] *Summer worker from the University of Toronto.*

dry film to the collimator, the edges of the film were painted with glyptal lacquer. The plutonium content of the source was $\backsim 4$ μgm. per sq. cm. and the collodion thickness was ~ 10 μgm. per sq. cm.

As the content of fissile material in this source was somewhat higher than that used previously and as the neutron flux available at the 4-in. experimental holes of the NRX pile was also increased, it was practicable to make use of an external beam from one of these holes. This arrangement was more convenient since an adjustment to the ionization chambers did not necessitate a pile shutdown. It was found, however, that higher field intensities in the chamber were required to produce saturation of fission fragment pulses. The field values required in this case were more in line with what was anticipated from α-particle measurements. The anomalously low fields required for saturation in the thermal column work are believed to result from the presence of a positive ion space charge arising from the much larger background ionization when the whole active volume of the chamber was irradiated.

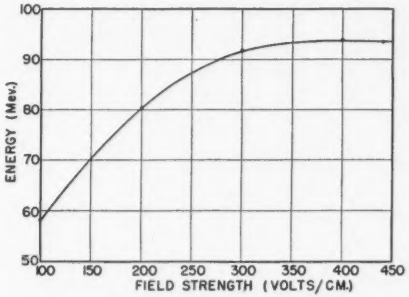

FIG. 1. *Saturation curve for fission fragments. Apparent energy of the light fragment maximum is plotted against the field strength in the collecting region, i.e., field in the cathode-grid space of the ionization chamber.*

The saturation curve of the light fragment peak is given in Fig. 1, which shows the apparent increase of energy of the light peak with the collecting field strength. Saturation occurs when the collecting field is sufficiently large to prevent columnar recombination. The operating field strength for subsequent measurements was 400 v. per cm., a value well above the "knee" of the saturation curve.

III. Experimental Results

The experiment was carried out in the same manner as the earlier work. For each fragment entering the collimated chamber a coincident partner appears in the uncollimated chamber. The fragment pulses from one chamber (say the uncollimated chamber) were passed into an electronic gate which allowed through only those pulses of a specific size (i.e., only fragments lying in a given energy interval). Subsequently, these pulses of selected energy were used to control a coincident gate through which pulses from the collimated

chamber were made to pass on their way to the pulse analyzer. Thus the pulses whose energy distribution was measured were created by those fragments in the collimated chamber whose partners in the uncollimated chamber were contained within the energy interval of the first gate.

Measurements were made, firstly, with the energy gate wide open so that coincidences were recorded between fragments of all energies. The resulting pulse analyzer distribution covered, of course, the whole fragment spectrum. This distribution, the usual double-humped curve, is shown in Fig. 2.

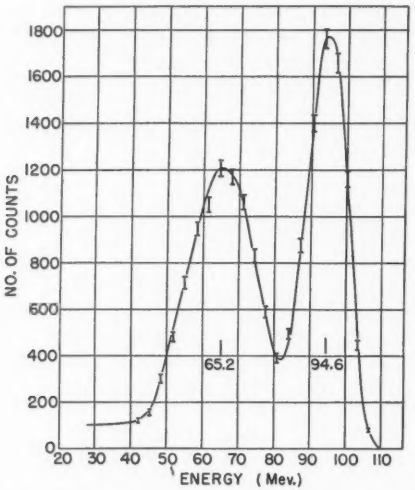

FIG. 2. *Spectrum of fragment energies for Pu^{239}. Distribution measured with the energy gate of the uncollimated chamber wide open.*

The energy gate was then narrowed to allow through only pulses in a 5 Mev. band. This band was moved progressively over the whole spectrum of Fig. 2 and in each case the coincident distribution was recorded. These "gated" runs are shown in Fig. 3 (*a–m*). The dotted curves are a reproduction of Fig. 2 on a reduced scale and indicate the positions of the gating band. The curves have been normalized to equal counting times and the standard deviations (of counting) are shown for the maxima only. The experimental measurements have been corrected for source and collimator losses in the same manner as for U^{235} and U^{233}. The collimator used was a 0.010 in. plate with many closely spaced 0.010 in. holes. The collimator correction was modified, however, by making measurements with large (0.125 in.) and small (0.010 in.) holed collimators both in 0.010 in. thick plates. These measurements indicated that the ionization loss in the collimator holes was not complete, and we have assumed that this loss was about half of the maximum, i.e., 0.7%. The source loss was in this case about 0.7%, giving a total error of $\sim 1.5\%$. The absolute cali-

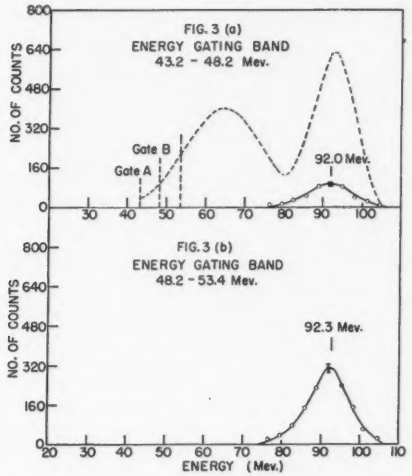

FIG. 3. (*a, b*) *Spectra for 5 Mev. gates centered at 45.7 and 50.8 Mev.*

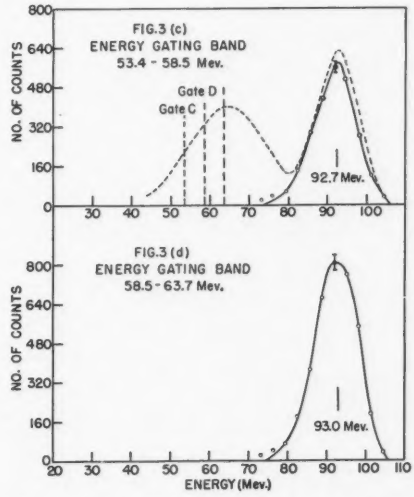

FIG. 3. (*c, d*) *Spectra for 5 Mev. gates centered at 55.9 and 61.1 Mev.*

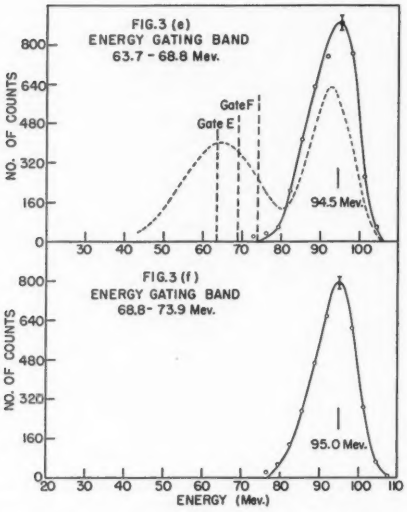

FIG. 3. (*e, f*) *Spectra for 5 Mev. gates centered at 66.2 and 71.4 Mev.*

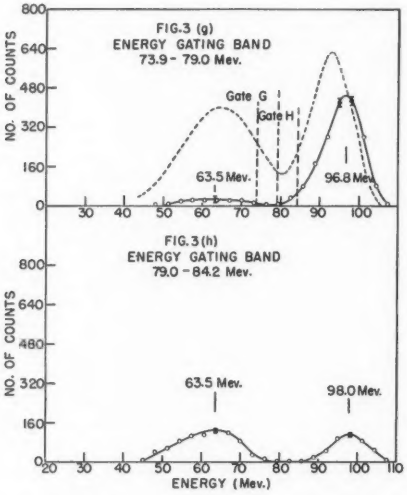

FIG. 3. (*g, h*) *Spectra for 5 Mev. gates centered at 76.5 and 81.6 Mev.*

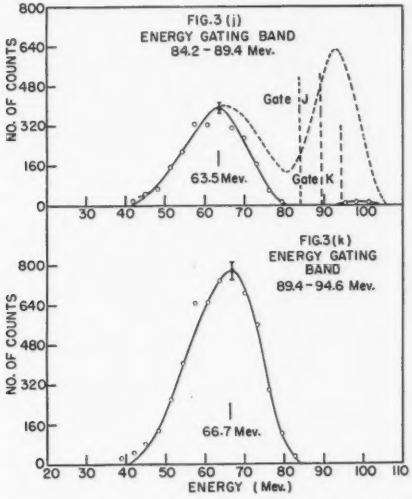

FIG. 3. (*j*, *k*) *Spectra for 5 Mev. gates centered at 86.8 and 92.0 Mev.*

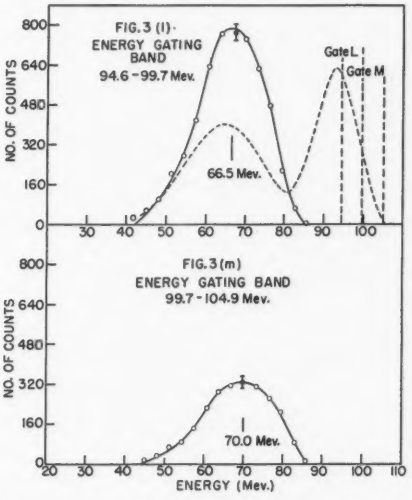

FIG. 3. (*l*, *m*) *Spectra for 5 Mev. gates centered at 97.1 and 102.3 Mev.*

bration was made by comparison with the Pu^{239} α-particles (energy = 5.159 Mev. (4)), and assuming that w, the number of electron volts per ion pair, was the same for fission fragments as for α-particles. The resultant corrected values are:

Most probable energy of light fragment = 94.6 Mev.
Most probable energy of heavy fragment = 65.2 Mev.

The corrected values have been used throughout in plotting the results.

IV. Discussion of Experimental Results

The wide spread of energies in the distribution of the gated runs, Fig. 3 (*a–m*), has been discussed in the previous paper (2). Fig. 3 (*e–g*) shows again that the minimum between the light and heavy fragment peaks of Fig. 2

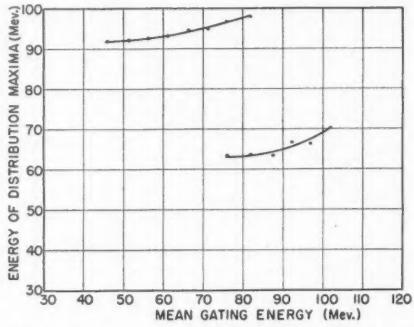

FIG. 4. *Variation of the most probable energy with the mean gating energy.*

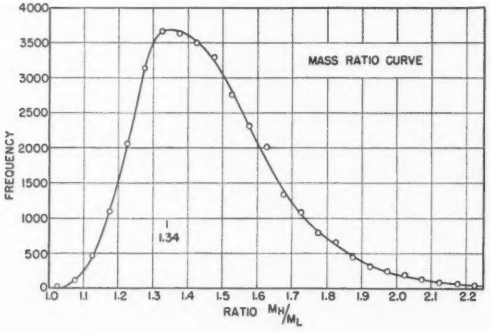

FIG. 5. *Mass ratio curve for Pu^{239}.*

does not represent the frequency of symmetrical fission even though the two distributions show a considerable overlap in this case. The derived curves of gating energy vs. energy of the corresponding maximum are shown in Fig. 4

and the mass ratio curve in Fig. 5. The mass distribution curve, Fig. 6, already published (3), is repeated here for completeness. The discrepancy between the mass distribution obtained from a coincident pulse experiment and that available from chemical identification (7) has already been discussed by the present authors (3). An interpretation in terms of neutron emission predominantly from the heavy fragment is still quite possible. However, the discussion of Brunton and Hanna (2) on this point favors an interpretation in terms of a difference in w. As pointed out in that discussion, a difference in w of 1 to 2%

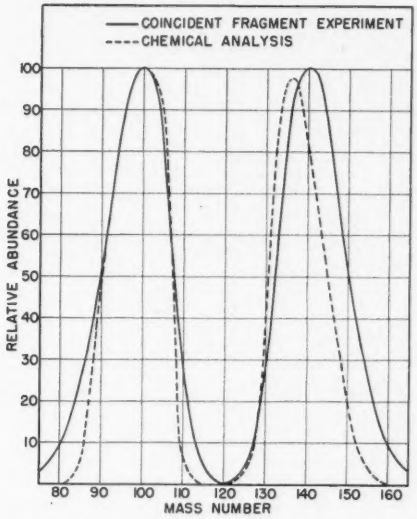

FIG. 6. *Mass curve for Pu^{239} from coincident pulse experiment and comparison with chemical curve.*

is quite reasonable, and this would be sufficient to remove any discrepancy in the present case.

Again for the sake of completeness, the contour diagram of the fission modes (3) is repeated as Fig. 7, and likewise a comparison of this experiment with the work of Deutsch and Ramsey (5) as Table I. In this table, the same correction for source and collimator losses has been applied to the measurements of Deutsch and Ramsey (5) as in the present work. This adjustment is thought to be justified since the source thickness and the collimator design were nearly identical in the two cases.

The most probable total kinetic energy as a function of mass ratio is shown in Fig. 8. The maximum in this curve is at a ratio of about 1.2 and is in excellent agreement with the work on fragment ranges by Katcoff, Miskel, and Stanley (6).

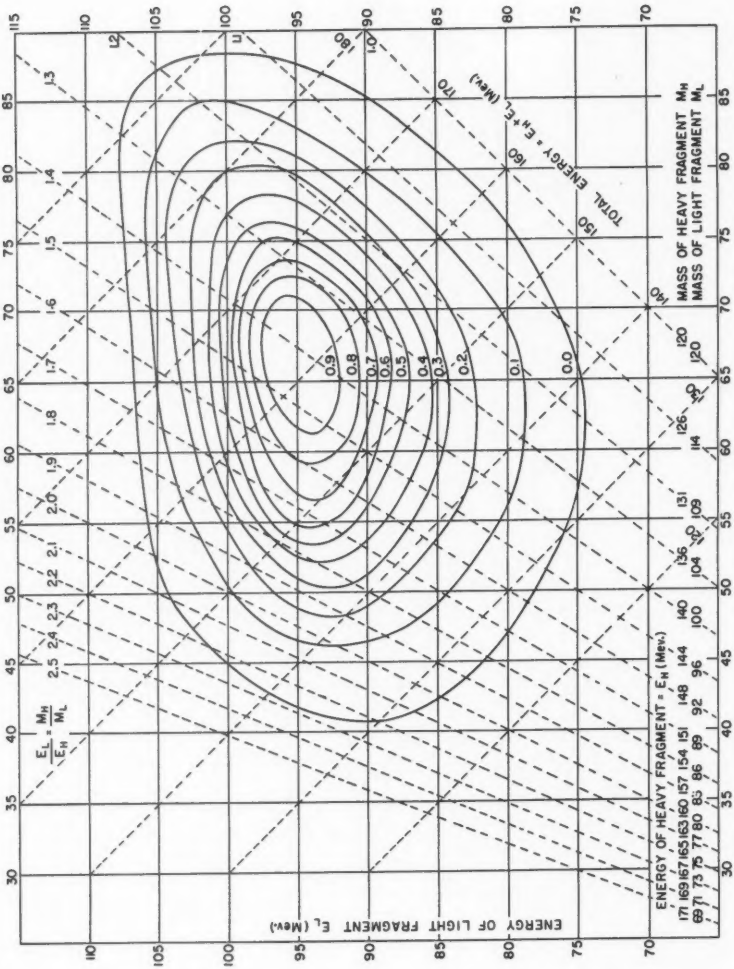
ENERGY OF LIGHT FRAGMENT E_L (Mev.)
$\frac{E_L}{E_H} = \frac{M_H}{M_L}$
TOTAL ENERGY = $E_H + E_L$ (Mev.)
ENERGY OF HEAVY FRAGMENT = E_H (Mev.)
MASS OF HEAVY FRAGMENT M_H
MASS OF LIGHT FRAGMENT M_L

FIG. 7. *Fission modes for Pu^{239}. Contours represent relative frequency of occurrence of the fission modes*

TABLE I

COMPARISON OF THE RESULTS OF THE PRESENT EXPERIMENT WITH THOSE OF DEUTSCH AND RAMSEY FOR FISSION IN Pu^{239}

Experimental quantity	Present* experiment	Deutsch* and Ramsey (5)
Most probable energy of light fragment, Mev	94.6	94.3
Most probable energy of heavy fragment, Mev	65.2	66
Ratio of most probable energies	1.45	1.43
Most probable mass ratio (from equal ratio interval curves)	1.34	1.32
Width at half-maximum of high energy peak, Mev	14	13
Width at half-maximum of low energy peak, Mev	24	21
Ratio of minimum to high energy peak, per cent	23	11
Ratio of peak heights	1.47	1.48

* *Values corrected for source and collimator losses.*

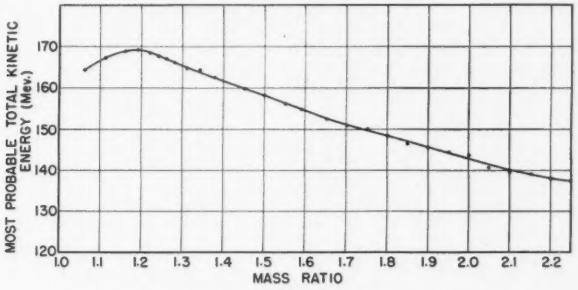

FIG. 8. *Variation of the most probable total kinetic energy with mass ratio.*

Finally, Table II gives a comparison of slow neutron fission in the three nuclides U^{233}, U^{235}, and Pu^{239}.

TABLE II

COMPARISON OF FISSILE NUCLIDES

Experimental quantity	U^{233}	U^{235}	Pu^{239}
Most probable energy of light fragment, Mev	93.0	94.5	94.6
Most probable energy of heavy fragment, Mev	56.6	60.2	65.2
Ratio of most probable energies	1.64	1.57	1.45
Most probable ratio (from equal ratio interval curves)	1.60	1.49	1.34
Width* of high energy peak, Mev	14	12	14
Width* of low energy peak, Mev	22	20	24
Width* of total energy curve, Mev	22	25	27
Width* of total energy curve for most probable mass ratio (from contour diagrams)	20	20	22
Mass ratio for most probable total energy	1.26	1.23	1.20

* *A half-maximum.*

Acknowledgments

The authors are greatly indebted to Mr. G. C. Hanna and Dr. B. W. Sargent for helpful advice and assistance.

References

1. BRUNTON, D. C. and HANNA, G. C. Phys. Rev. 75: 990. 1949.
2. BRUNTON, D. C. and HANNA, G. C. Can. J. Research, A, 28: 190. 1950.
3. BRUNTON, D. C. and THOMPSON, W. B. Phys. Rev. 76: 848. 1949.
4. CRANSHAW, T. E. and HARVEY, J. A. Can. J. Research, A, 26: 243. 1948.
5. DEUTSCH, M. and RAMSEY, M. Declassified document MDDC-945: Mass ratios and energy release in fission of U^{235} and Pu^{239} by thermal neutrons. United States Atomic Energy Commission. 1946.
6. KATCOFF, S., MISKEL, J. A., and STANLEY, C. W. Phys. Rev. 74: 631. 1948.
7. STEINBERG, E. P., SEILER, J. A., GOLDSTEIN, A., and DUDLEY, A. Declassified document MDDC-1632: Fission yield in uranium^{233}. United States Atomic Energy Commission. 1947.

THE VELOCITY OF SOUND IN HELIUM AT TEMPERATURES −78°C. TO 200°C. AND PRESSURES UP TO 70 ATMOSPHERES[1]

By W. G. Schneider and G. J. Thiessen

Abstract

The velocity of sound in pure helium gas has been measured as a function of pressure at −78°, 0°, 50°, 100°, and 200°C., using an ultrasonic interferometer of the double crystal type. From the sound velocity data second virial coefficients were obtained, and the ratio of specific heats was derived as a function of pressure.

Introduction

The velocity of sound in a gas is given by

$$U = \left[-\frac{\gamma V^2}{M} \left(\frac{\partial P}{\partial V} \right)_T \right]^{\frac{1}{2}} \tag{1}$$

where U = velocity of sound in centimeters per second,
γ = specific heat ratio, C_p/C_v,
V = volume in cubic centimeters per mole,
P = pressure in dynes per square centimeter,
M = molecular weight in grams per mole.

Accordingly, velocity of sound data can be employed to obtain specific heat data and/or compressibility data. If the equation of state of a gas is known, then, from measurements of the sound velocity as a function of temperature all the usual thermodynamic properties of the gas can be derived. The following report describes some measurements of the velocity of sound in helium in the temperature range from −78°C. to +200°C. The measurements were also carried out as a function of pressure, partly as a check on the compressibility measurements of helium previously reported (6) and partly to investigate the possibility of using sound velocity data to obtain both compressibility data and specific heat data. The latter method would at first sight appear to offer the advantage of requiring only a small sample of gas and avoiding the necessity of bothersome "dead-space" corrections encountered in most of the conventional methods for measuring gas compressibility. Van Itterbeek and coworkers (7), in a series of papers, have attempted to obtain the second virial coefficient B as a function of temperature for several gases from the variation of sound velocity with temperature and pressure and in addition two or three known values of B, which were obtained from the usual compressibility isotherm measurements. In the following report a somewhat similar analysis, which does not require any values of B to be known, is presented.

1. *Manuscript received April 27, 1950.*
Contribution from the National Research Council Laboratories, Ottawa, Canada. Issued as N.R.C. No. 2185. Presented in part at Canadian Institute of Chemistry Conference, Toronto, June 1950.

Experimental

The Acoustic Interferometer

The velocity of sound measurements were made with an ultrasonic interferometer designed for use over a wide temperature range and pressures up to 100

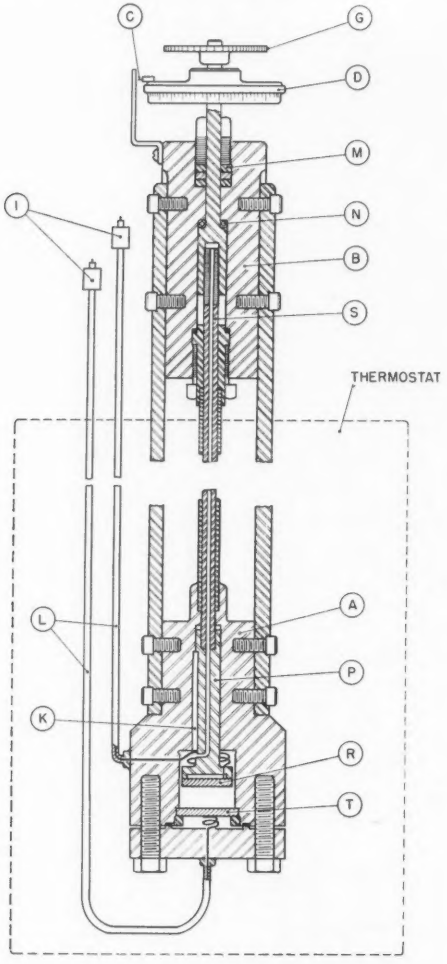

FIG. 1. *Acoustic interferometer.*

atm. The interferometer shown schematically in Fig. 1 was a modification of a high pressure interferometer described by Hodge (2). The acoustic chamber, *A*, which could be immersed in an accurately controlled thermostat at any

desired temperature, was separated by an extension from the body B, which houses the metric screw and the pressure packing. This design protected the latter from the extreme temperatures to which the acoustic chamber could be subjected.

The interferometer was of the double crystal type. The receiving quartz crystal R, which also serves as the reflector, was mounted on a keyed movable piston P, joined to the screw in the body B. By means of a synchronous motor attached to the screw through a worm gear drive G, the receiving crystal could be moved up or down in the acoustic chamber at a steady and uniform rate. The signal from the receiving crystal was amplified and automatically recorded

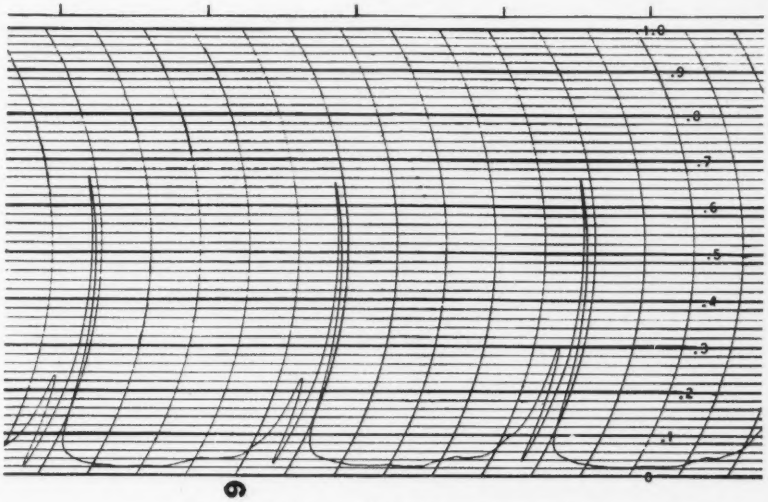

FIG. 2. *Typical record showing resonance peaks.*

on an Esterline Angus pen recorder. To transfer the distance scale (of the reflector) on to the paper record, a marginal chronograph pen of the recorder was actuated at each revolution by means of an electric contact C mounted on the graduated drum D. A typical record showing several resonance peaks of the interferometer is reproduced in Fig. 2. The distance scale as recorded by the chronograph pen is shown on the upper margin. Since the screw was cut with a metric thread containing 20 threads per cm., each revolution, represented by two successive marks of the chronograph pen, corresponds to a movement of the reflector (receiving crystal) of 0.05 cm. The reflector and the paper of the recorder were driven at rates which gave a magnification of the distance scale on the paper record of 140×. Accordingly the distance between resonance peaks on the paper record could be measured with sufficient accuracy with a good centimeter rule.

The transmitter crystal T, which was matched in frequency to the receiver crystal, was mounted on a shoulder at one end of the chamber and held in place by a crimped spring, made of Inconel X, and a threaded retainer ring. The crystal leads were brought outside the thermostat through 1/32 in. bore steel capillaries L, and terminated in the electrically insulated pressure seals I. The resonance frequency of the crystals was 600 kc. This frequency altered by some 2 or 3 kc. owing to the mounting and the temperature to which the acoustic chamber was subjected. Accordingly a variable oscillator (General Radio Co.) was employed to drive the transmitter crystal, and the frequency was adjusted to its optimum value for each experiment.

As shown in Fig. 2 the resonance peaks exhibit a small satellite peak, whose position relative to the main peak depended somewhat on the frequency and the position of the reflector in the acoustic chamber. The cause of this satellite peak could not be traced.

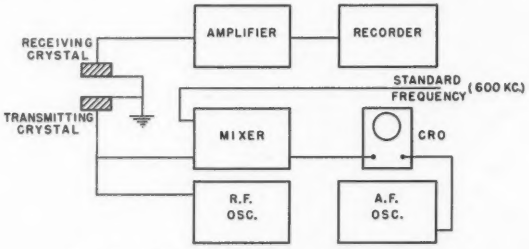

FIG. 3. *Block diagram of measuring apparatus.*

The frequency of the transmitter crystal was measured by comparing it with a standard 600 kc. frequency signal lead into the laboratory by cable from the Standard Frequency Laboratory of the NRC Radio Division. The difference frequency was measured by comparison with a low drift audio oscillator (Hewlett Packard). Fig. 3 shows a block diagram of the driving and measuring apparatus.

Procedure

The purification of the helium, the thermostat, and the free piston gauge for pressure measurements have been described previously (5, 6). Temperatures were measured by a platinum resistance thermometer and are estimated accurate to ± 0.01°C. The temperature at -78°C., which was obtained by using a rapidly stirred mixture of powdered dry ice and alcohol, varied slightly from day to day by as much as 0.2°, but during the course of the measurements on any one day remained steady to within 0.02°C. The mean temperature of all the measurements was -78.11°C.

To carry out the velocity of sound measurements pure helium was compressed into the interferometer, which had previously been thoroughly evacuated and flushed, and a series of sound velocity measurements were taken at

pressures from approximately 70 atm. down to 6 atm. Successive pressures were obtained by bleeding off a portion of the gas. The pressure, as measured by the free piston gauge, varied slightly as the receiving crystal was moved from one end of the chamber to the other. (This is due to the dead space in chamber B being at room temperature instead of the thermostat temperature.) Accordingly the pressure was balanced before and after the traverse of the receiving crystal and the mean pressure was taken. Likewise in measuring the records the average distance between peaks, i.e., the half wave length, was obtained by measuring the distance between the first and last peak and dividing this distance by the number of peaks (usually 10 to 14 depending on the temperature). The mean frequency, which varied not more than ± 30 cycles during a complete traverse of the crystal, was also recorded at each pressure. From the frequency and the mean wave length as measured with the aid of the distance scale recorded by the chronograph pen, the velocity at each pressure was computed.

Some difficulty was encountered in the use of the interferometer at 200°C. The acoustic chamber and the piston P were machined from stainless steel, and the piston P was lapped to a good fit with a clearance of only 0.001 in., to ensure proper alignment of the two crystals. At 200°C. the piston which was not lubricated was found to score and seize, even after the clearance had been increased to 0.0025 in. The difficulty was finally overcome by the use of an invar piston with 0.003 in. clearance. To use this type of interferometer at temperatures above 200°C. would require some modification, as for example the use of hardened steel, having a low expansion coefficient, for both the acoustic chamber and the piston.

Results

(1) *Velocity of Sound as a Function of Pressure*

Since over the pressure range employed in these experiments the PV isotherms of helium are linear with pressure we can use the simple virial equation

$$PV = A + BP. \tag{2}$$

Substitution in Equation (1) leads to

$$U = \sqrt{\frac{\gamma A}{M}}\left(1 + \frac{B}{A}P\right). \tag{3}$$

Here γ is not a constant but varies with pressure. From well known thermodynamic relations and Equation (2) it can be shown (3) that to a sufficiently good approximation

$$\gamma = \gamma_0\left[1 + \frac{4}{3R}\left(\frac{dB}{dT} + \frac{T}{5}\frac{d^2B}{dT^2}\right)P\right]. \tag{4}$$

Combining Equations (3) and (4) we obtain

$$U = U_0\left[1 + \frac{1}{R}\left(\frac{B}{T} + \frac{2}{3}\frac{dB}{dT} + \frac{2}{15}T\frac{d^2B}{dT^2}\right)P\right], \tag{5}$$

where $$U_0 = \sqrt{\frac{\gamma_0 A}{M}}. \tag{6}$$

Thus a plot of the sound velocity against pressure should give the zero-pressure sound velocity U_0 as the intercept, and the slope of the plot is related to the second virial coefficient. Table I contains a summary of the sound velocity measurements. In the second and third columns the zero-pressure velocity obtained from the experimental plots is compared with the corresponding values calculated from Equation (6). From the experimental value of U_0 the zero-pressure heat capacity ratio, γ_0, was calculated for each temperature. These are shown in column 4. Column 6 shows the slopes of the velocity–pressure plots, and column 7 the number of runs carried out at each temperature, each run consisting of eight or more velocity measurements more or less evenly spaced along the pressure axis. The results of one run at 0°C. are shown plotted in Fig. 4.

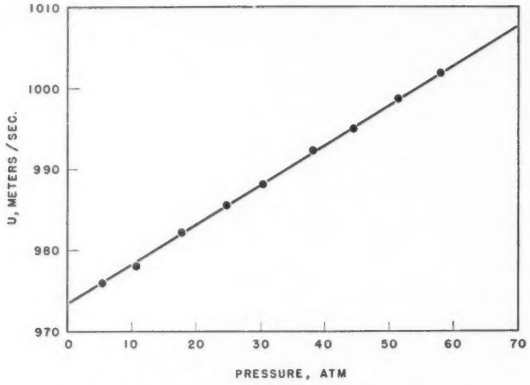

FIG. 4. *Plot of velocity of sound vs. pressure at 0°C.*

The experimental zero-pressure velocities are in every case higher than the calculated values and give rise to slightly higher values of γ_0 than the theoretical value of 1.6667. The estimated error in the velocity measurements is approximately ± 1.0 m. per sec. or approximately 0.1%. The error in the frequency measurement and in the screw thread of the interferometer is considerably less than this. The probable error in the slope of the sound velocity – pressure plots is about 1.0%. At the bottom of Table I some measurements carried out by Hodge (2) at 27°C. are shown for comparison. His large error in the zero-pressure velocity U_0 can probably be attributed to impurities in the helium gas used in the measurements. Because of the small density of helium, the sound velocity is very sensitive to the presence of a few per cent of a heavier gas such as nitrogen.

TABLE I

SUMMARY OF SOUND VELOCITY MEASUREMENTS IN PURE HELIUM

Temperature, °C.	U_0, m./sec.		γ_0		Slope $\left(\frac{dU}{dP}\right)_T$	No. of runs
	Expt.	Calc.	Expt.	Theor.		
−78.11	822.5	821.8	1.669_6	1.6667	0.603	4
0	973.9	972.5	1.671_5		0.486	4
50	1059.6	1057.8	1.672_4		0.443	3
100	1138.4	1136.7	1.671_6		0.402	7
200	1280.9	1279.9	1.669_2		0.343	7
27.0 (Hodge)	945.3	1019.5	1.443		0.454	

In Fig. 5 the velocity–pressure data at each temperature are shown graphically in the form:

$$U/U_0 = 1 + 1/U_0\left(\frac{dU}{dP}\right)_T P \tag{7}$$

Fig. 6 is a plot of the slope $\left(\frac{dU}{dP}\right)_T$, listed in column 6 of Table I, as a function of temperature.

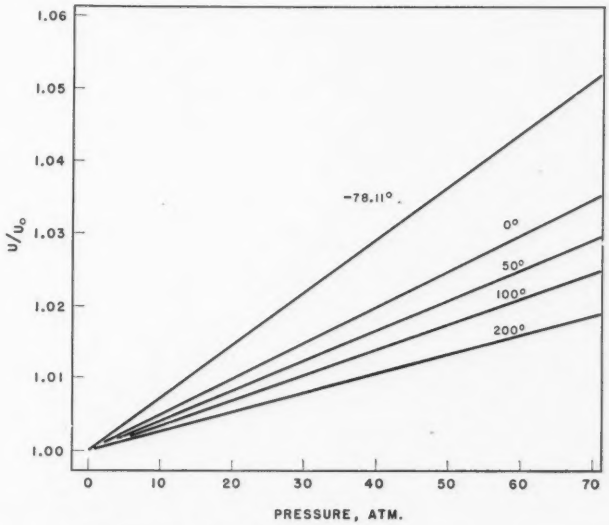

FIG. 5. *Plot of sound velocity ratio U/U_0 vs. pressure.*

(2) *The Specific Heat Ratio, γ, as a function of Pressure*

Method I.—If the second virial coefficient, B, is known at each temperature, then with the aid of Equation (3) γ can be computed as a function of pressure from the sound velocity data.

Method II.—If the second virial is accurately known as a function of temperature so that the first and second derivatives can be evaluated, the pressure coefficient of γ can be computed directly from Equation (4). For this method

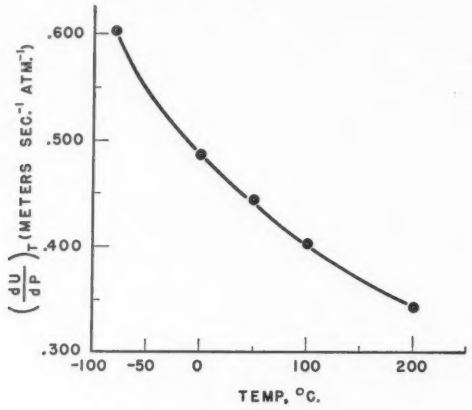

FIG. 6. *Plot of the slope* $\left(\frac{\partial U}{\partial P}\right)_T$ *vs. temperature.*

we have used two alternative functions which at present appear most reliable in our temperature range:

$$(a)\ B_T = 10^{-3}\left[0.5485 - 0.1315 \times 10^{-3}T + \frac{3.754}{T}\right], \tag{8}$$

where T is in degrees Kelvin.

This function had been fitted to recent experimental measurements reported by one of us (6) and is valid in the temperature range 0° to 600°C.

$$(b)\ B_T = 0.76 \times 10^{-5}\left[84.78 - 3.54 \times 10^{-2}T - \frac{15.25}{T} \times 10^{2} - \frac{0.210}{T^3} \times 10^{6}\right]. \tag{9}$$

This function, reported by Holborn and Otto (4), was fitted to experimental measurements over the temperature range −258° to +400°C.

The results of the computations, shown in Table II, are expressed in terms of the pressure coefficient α, defined by

$$\gamma = \gamma_0 - \alpha P. \tag{10}$$

In view of the fact that for helium α is a very small quantity, the agreement in the results calculated by the two methods can be considered satisfactory. Moreover it will be noted that method II does not depend on sound velocity measurements, but only on the equation of state. Accordingly the results of Table II provide a valuable check on the internal consistency of the equation of state data for helium, i.e., the second virial coefficient. The Holborn and

Otto relation for B [Equation (9)] gives rise to an increase in α with temperature above 0°C. and is therefore inadequate in this temperature range, where it predicts a curvature of the B vs. T plot which is concave downward, whereas a plot of Equation (8) in the same temperature range has a curvature concave upward.

TABLE II

DERIVED VALUES OF THE PRESSURE COEFFICIENT IN THE RELATION $\gamma = \gamma_0 - \alpha P$

Temperature, °C.	$\alpha \times 10^5$ (atm.$^{-1}$)			
	Method I	Method II		Clark and Katz
		a*	b**	
−78.11	4.0	. .	5.2	
0	8.6	9.8	10.7	
23.1				20.0
50	6.0	9.3	12.3	
100	6.1	9.0	13.3	
200	5.7	8.6	14.4	

* *Calculated from Equation (8).*
** *Calculated from Equation (9).*

Included in Table II for comparison is a value of α at 23.1°C. obtained by Clark and Katz (1) by a low frequency resonance method. This value is roughly a factor of two greater than the corresponding values obtained by the present methods.

(3) *Derivation of B as a Function of Temperature from Sound Velocity Data*

If the sound velocity as a function of pressure has been measured at a number of different temperatures, then according to Equation (4) one can, in principle at least, deduce the second virial B as a function of temperature from the slopes of the sound velocity – pressure plots (see Fig. 6 and Table I, column 6). Equation (5) can be written

$$U = U_0(1 + sP), \tag{11}$$

where

$$s = \frac{1}{U_0}\left(\frac{dU}{dP}\right)_T = \frac{1}{R}\left(\frac{B}{T} + \frac{2}{3}\frac{dB}{dT} + \frac{2}{15}T\frac{d^2B}{dT^2}\right). \tag{12}$$

To obtain B as a function of temperature requires the solution of the differential equation (12). Since this is not easily accomplished the following indirect method was used. Define a function $S(T)$ by

$$S(T) = sRT = sA$$

and hence

$$S(T) = B + \frac{2}{3}T\frac{dB}{dT} + \frac{2}{15}T^2\frac{d^2B}{dT^2}. \tag{13}$$

From the experimental slopes of the sound velocity vs. pressure plots, $S(T)$ can be calculated at each temperature and plotted as a function of temperature.

An inspection of this plot will suggest a functional relation for $S(T)$. The following function was chosen.

$$S(T) = K + LT + \frac{M}{T}, \tag{14}$$

and the coefficients were evaluated from the experimental data by least squares fitting. Since in Equation (13) the power of T in each term is the same as the order of the differential, it follows that $B(T)$ must have the same form as $S(T)$ or

$$B(T) = a + bT + \frac{c}{T}. \tag{15}$$

Then by evaluating the first and second derivatives of (15), substituting in (13) and comparing with (14) we have

$$a = K, \quad b = \frac{3L}{5}, \quad c = \frac{15}{9}M.$$

Evaluating the coefficients in this manner we obtained:

$$B(T) = 10^{-3}\left[0.5146 - 0.0808 \times 10^{-3}T + \frac{11.03}{T}\right]. \tag{16}$$

TABLE III

COMPARISON OF SECOND VIRIAL COEFFICIENTS FOR HELIUM

Temperature, °C.	Second virial coefficient. $B \times 10^3$ (Amagat units)		
	From sound velocity		From compressibility data
	Using Equation (16)	Using Equation (17)	
−78.11	0.552	0.544	..
0	0.530	0.531	0.525
100	0.512	0.516	0.509
200	0.498	0.502	0.494

Table III shows a comparison of the second virials given by (16) with the values obtained from compressibility measurements as summarized by Equation (8). The agreement above 0°C. is rather better than could reasonably be expected, particularly since the true second virial curve is apparently slightly S-shaped in the temperature range −78° to +200°C. and Equations (14) and (15) would require some modification. For this reason also the value at −78.11°C., which will be affected most, is somewhat too high. The present data, however, are not sufficiently extensive to warrant a closer fitting, and to illustrate this the above was repeated using the following form for $S(T)$.

$$S(T) = K + LT + MT^2.$$

This will of course lead to a similar equation for $B(T)$ so that

$$B(T) = a + bT + cT^2, \tag{17}$$

where the coefficients have the values $a = 5.807 \times 10^{-4}$, $b = -2.022 \times 10^{-7}$, $c = 0.741 \times 10^{-10}$. The resulting values for $B(T)$ are listed in Table III in the third column. It is obvious that it is impossible, on the basis of present data, to choose between Equations (16) and (17).

In conclusion, it may be stated, on the basis of the present measurements, that the sound velocity method of obtaining equation of state data is comparable in accuracy to the usual compressibility methods, provided the data are taken at sufficiently close temperature intervals, and the temperature range, for which an analysis such as that presented above is applied, is not too extensive. The latter statement is probably no real objection to the method, since the same difficulty in fitting, for example, the second virial coefficient over a wide temperature range to a single function is also common to the compressibility methods (cf. Equations (8) and (9)). The acoustic method is perhaps somewhat more difficult to carry out experimentally, and, with present techniques at least, does not appear to offer any advantage over the direct compressibility measurements. When available, however, the acoustic data provide a valuable check on the compressibility data.

The above method, which applies to gases with linear isotherms, can easily be extended to gases giving rise to parabolic isotherms, and Equation (11) then becomes

$$U = U_0(1 + sP + kP^2),$$

an equation which has been extensively applied by Van Itterbeek and coworkers (7). The coefficients can be obtained by a least squares fit to the experimental data, and, as before, s is given by Equation (12) from which the second virial coefficient as a function of temperature can be derived. The coefficient k is related to the second and third virial coefficients and their derivatives and is not amenable to a simple analysis.

References

1. Clark, A. L. and Katz, L. Can. J. Research, A, 21: 1. 1943.
2. Hodge, A. H. J. Chem. Phys. 5: 974. 1937.
3. Keesom, W. H. Helium. Elsevier Publishing Co. Inc., Amsterdam. 1942. p. 95.
4. Otto, J. Handbuch der experimental physik, Bd. 8, Teil, 2, p. 79. Akad. Verlag. Leipzig. 1929.
5. Schneider, W. G. Can. J. Research, B, 27: 339. 1949.
6. Schneider, W. G. and Duffie, J. A. H. J. Chem. Phys. 17: 751. 1949.
7. Van Itterbeek, A. and Van Doninck, W. Proc. Phys. Soc. (London), 58: 615. 1946. (References to earlier work by the same authors are given in this paper.)

A CALORIMETRIC MEASUREMENT OF THE DISINTEGRATION RATE OF A P^{32} SOURCE[1]

By J. G. Bayly

Abstract

The calorimetric method of measuring sources is of value when the average energy per disintegration is known, and may be used to check the accuracy of an "absolute" beta counting technique. This paper describes a differential calorimeter designed for this type of measurement, and an experimental determination of the disintegration rate of a P^{32} source. The calorimetric measurement gave a value of the disintegration rate with a probable error of 0.7% differing by 1.8% from the result obtained from an absolute count of the β-activity. The absolute count was accurate to $\pm 2\%$. The calorimeter has a sensitivity limit of less than 10μw., and makes use of thermistors to measure temperature changes of the order of 10^{-3}°C.

Introduction

In spite of notable improvements in the techniques, absolute counts of β-particles per unit time and hence disintegration rates are still subject to errors* of as much as 10%, particularly in cases such as I^{131}, where the disintegration scheme is complex, and in cases such as P^{32}, where no γ-ray is emitted and coincidence counting cannot be used.

The calorimetric method of measuring the disintegration rate of a source of β-particles is valuable when the average energy per disintegration is accurately known from the shape of the β-spectrum. This paper describes a calorimeter designed for this type of measurement and an experimental determination of the disintegration rate of a P^{32} source. The derived disintegration rate is used to check the accuracy of an absolute β-counting method used in this laboratory.

The source of P^{32} was made by irradiating red phosphorus in the NRX pile. The heat output was measured over several weeks. Afterwards the β-particles emitted in a known solid angle were counted, using a known fraction of the source. The two measurements of disintegration rate agree within their total probable errors (2%).

Calorimeter

The calorimeter developed for measuring the energy released per second by sources of β-particles may be described as a differential, or twin, calorimeter of the nonisothermal, nonadiabatic type. It is capable of detecting less than 10^{-5} w., and may be used with sources producing as much as 10^{-2} w. The heat

[1] *Manuscript received March 8, 1950.*
Contribution from the Nuclear Physics Branch, Atomic Energy Project, National Research Council of Canada, Chalk River, Ont. Issued as N.R.C. No. 2187.

* *Measurements on I^{131} by the National Bureau of Standards, Washington, D.C., are believed to have an accuracy of $\pm 5\%$, but an intercomparison of absolute counting rates made on samples distributed April 15, 1949, showed that of 41 laboratories participating, only 50% obtained values within $\pm 7\%$ of the mean value. The spread of values obtained in a P^{32} intercomparison (samples distributed Feb. 23, 1949) was slightly greater, with 50% of the results more than $\pm 10\%$ from the most probable value.*

produced by the source in its calorimeter is measured by comparing it with the amount of electrical power required to produce the same temperature rise in an essentially identical calorimeter. Temperature changes are detected by means of thermistor resistance thermometers.

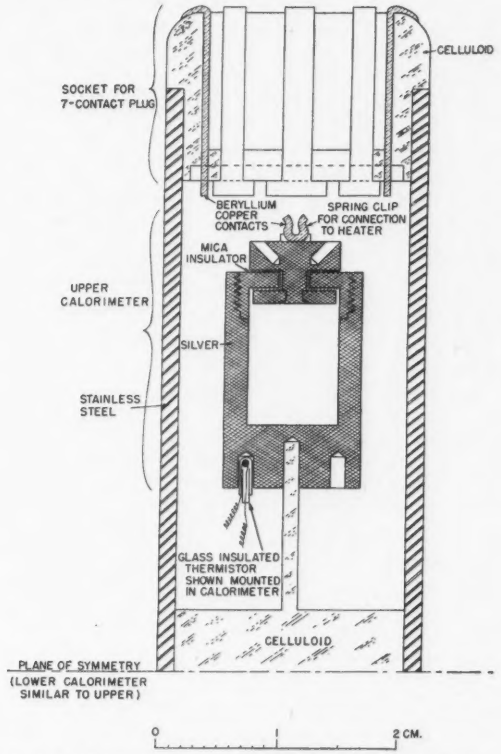

FIG. 1. *Upper half of differential calorimeter. The lower half is identical, with the thermistor bridge leads (not shown) passing through the central celluloid support.*

The differential calorimeter consists of two silver capsules symmetrically located in a constant temperature shield, as shown in Fig. 1. The temperature of the shield is controlled by a thermal filter, which attenuates the fluctuations in room temperature so that only very slow drifts in the shield temperature are possible. This type of shield, first recommended by Tian (6), is very suitable for calorimetric work with radioactive sources where the actual temperature does not affect the heat produced but where rapid changes in temperature are undesirable.

The temperatures of the two calorimeters are compared by means of thermistors embedded in their thick bases. It is qualitatively apparent that the

temperature observed at one end of the container depends not only on the amount of heat being liberated in the capsule but also on the spatial distribution of the source of heat. An approximate calculation shows that, owing to the high conductivity of silver, this effect is very small. Even with all the heat dissipated at one end of the capsule the temperature rise of the thermistors differs by less than 0.5% from the rise when the same amount of heat is dissipated uniformly. Since both the source and the electric heater are approximately of the same size and must produce very similar temperature distributions, the error introduced by this effect is negligible.

The resistance thermometer circuit differs from that used by Rutherford and Robinson (4) in that all four arms of the bridge are thermally sensitive. Each calorimeter determines the temperature of two opposite arms. In addition to doubling the sensitivity, this method of construction improves the stability of the circuit, since the wires connecting the arms of the bridge are all short and are at the temperature of the calorimeter, rather than long and at the fluctuating room temperature.

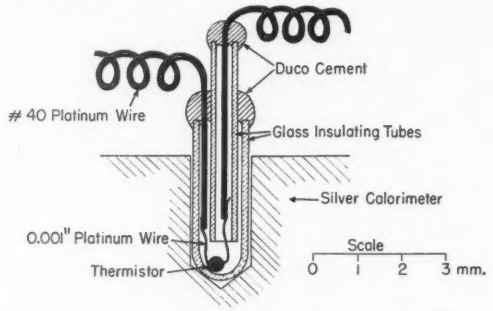

FIG. 2. *Method of insulating thermistors for mounting in the calorimeter bases.*

Western Electric D 170575 thermistors were used as the resistance thermometers. These units have a resistance of approximately 2000 ohms at room temperature, a temperature coefficient of resistance roughly -10 times that of platinum, and are very small. The thermistor beads with their glass coatings are approximately 0.05 cm. in diameter, and the leads are made of 0.001 in. platinum. The method of insulating the leads for insertion in the holes in the calorimeter is shown in Fig. 2.

The voltage across the thermistor bridge, Fig. 3, was maintained at 0.190 v. A Leeds and Northrup 2290 Type HS galvanometer was used to detect bridge unbalance. The voltage sensitivity of the galvanometer, measured with its critical damping resistor connected, was 0.35 μv. per mm. using a folded light path of 4 m.

The calorimeter was tested by applying heat from resistors inserted in the two calorimeters. The power dissipated in each calorimeter was found by

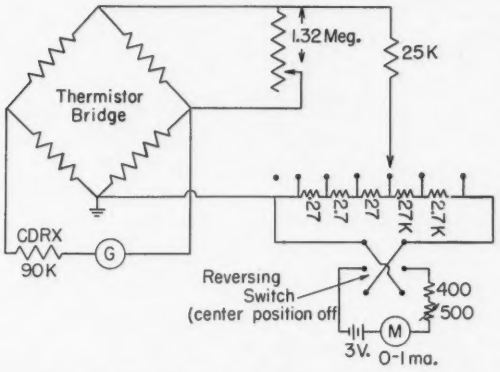

FIG. 3. *Thermistor bridge and associated circuits.*

measuring both current and voltage. The calibrating circuit is shown in Fig. 4. The resistors were guaranteed accurate to 0.05%, and, when checked on a Wheatstone bridge, showed variations from their nominal values of less than $\pm 0.015\%$. The voltages were measured by a potentiometer and standard cell with a limiting error of 0.0004 v. Following engineering practice (2) the probable error will be taken as 1/3 the limiting error, or ± 0.00015 v., and for the resistors, 0.02%. For a typical measurement, the voltage measured was 0.45 v., or the error in the voltage was $\pm 0.033\%$. The power measurement then had a probable error of $\pm\sqrt{(0.02)^2 + (2 \times 0.033)^2}$ or $\pm 0.07\%$.

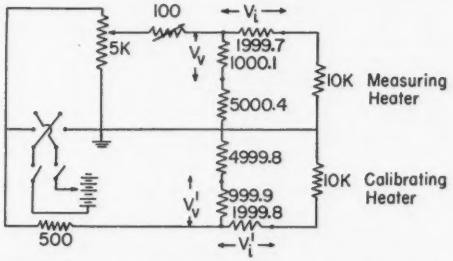

FIG. 4. *Calibrating and power measuring circuits. The power supplied to each heater is found by measuring the voltages V_v and V_i. The calibrating heater is removed when the source is inserted.*

This test indicated that the heat leakage from the upper calorimeter was $3.8 \pm 0.2\%$ greater than from the lower.

The radiophosphorus was inserted in the upper calorimeter. Electrical energy was supplied to a resistor in the lower calorimeter, and adjusted daily to keep the galvanometer near zero. To eliminate errors due to zero drift and thermal e.m.f.'s in the connecting wires, the voltage across the thermistor

bridge was reversed, and the double deflection of the galvanometer measured. The temperature sensitivity was 6×10^{-5} °C. per mm. of double deflection.

Calorimeter Shield

The calorimeter shield, shown in Fig. 5, is essentially a thermal filter consisting of two concentric shells of water insulated from each other and from the room by layers of rock wool. Assuming that a cylindrical shell with its height approximately equal to its diameter, covered at each end by a disk of thickness equal to the cylindrical wall thickness, may be treated as a spherical shell, an approximate mathematical analysis of the shield is possible.

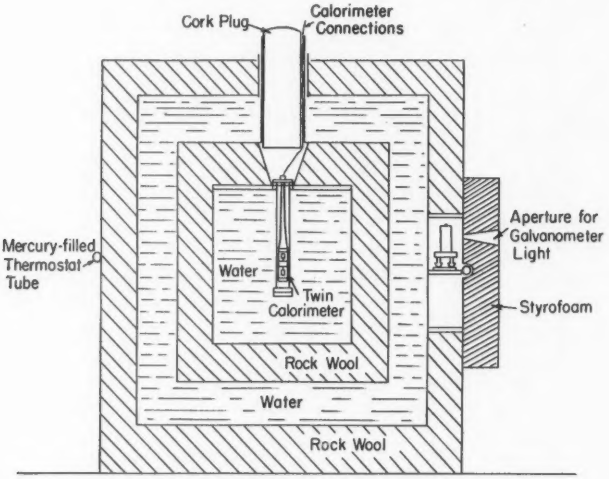

FIG. 5. *Calorimeter shield.*

There are two water walls, of outer radii r_1 and r_3, and two rock wool walls, outer radii r_2 and r_4, where $r_1 < r_2 < r_3 < r_4$. The largest radius r_4 was determined by the space available for the apparatus. Then the attenuation for a thermal fluctuation of duration short compared with the time constant of each water shell with its surrounding insulating layer was made a maximum by making

$$r_1/r_2 = 2/3;\ r_2/r_3 = (2/5)^{\frac{1}{2}};\ r_3/r_4 = 4/5;$$

or

$$r_1 : r_2 : r_3 : r_4 = 0.4 : 0.6 : 0.8 : 1.0.$$

Assuming the thermal conductivity of rock wool to be 10^{-4} cal. per cm.^{2} per °C. per cm. per sec., the filter reduces the amplitude of daily temperature fluctuations by a factor of the order of 3000.

The room in which the calorimeter is located was maintained at a temperature constant to ±0.05°C. The thermostat consists of a mercury-filled stainless steel tube, wrapped around the outside of the calorimeter shield, terminated by a 1.5 mm. glass capillary in which a nickel wire (0.006 in. diam.) makes contact with the mercury surface if the temperature rises. To retain reliable action the space above the mercury is filled with argon and the current broken by the contact is limited to 3 μa. The thermostat, through its amplifier and power relay, controls the heat supplied by a resistance heater distributed around the walls of the room near the floor.

In order to avoid trouble with the galvanometer circuits, care was taken to minimize leakage currents, stray magnetic fields, and thermal gradients. Leakage currents, even though they originate from circuits carrying alternating current, can disturb a sensitive galvanometer by being rectified by a nonohmic surface resistivity. Effects due to leakage were made negligible by shielding all the leads and enclosing the room heater in a grounded wire screen. Stray magnetic fields and thermal gradients are troublesome only if they vary with time.

The latter effects are reduced greatly by making the heat supply to the room change slowly. This is accomplished by means of a motor-driven variable transformer: when the thermostat demands more heat, a relay causes the motor to increase the voltage applied to the heater; and when the temperature has risen enough to satisfy the thermostat, the relay reverses the motor. In this way the heat supply is made to hunt with a 10 min. period back and forth across the demanded value. If the demanded power changes, as for example when the heat loss through the walls of the room increases owing to a reduction in the temperature outside, the motor runs for a slightly longer time in one direction than the other until the mean heat supply again coincides with the new demanded value. This method of control avoids the sudden large fluctuations of power characteristic of a simple on–off system and yet provides a much greater range of heat inputs than can be obtained by switching a small fraction of the total power.

The temperature of the outer jacket of the calorimeter shield is monitored continuously by means of four Western Electric Type 4A thermistors, connected in series parallel, distributed over the outer surface of the jacket. These thermistors, shunted by an adjustable 1250 ohm rheostat, replace the thermohm of a Leeds and Northrup Micromax recorder. The slide wires of the Wheatstone bridge in the Micromax are shunted to reduce the over-all resistance by about 10, giving a corresponding increase in sensitivity. Since the thermistors have a temperature coefficient approximately 10 times that of the thermohm, the final sensitivity is approximately 100 times greater than the sensitivity of the unmodified Micromax. The original range of the instrument was from −30°C. to +50°C. with 1°C. divisions, while the final range is 0.8°C., with 0.01°C. divisions.

Heat Produced by P^{32}

Radiophosphorus is particularly suitable for calorimetric measurements because:

(1) It emits no nuclear γ-radiation, thus simplifying the correction for energy escaping from the calorimeter.

(2) It can be produced with a high watts per gram ratio in the NRX pile.

(3) Its β-spectrum is well known.

A similar experiment on P^{32}, produced by the irradiation of S^{32}, has been made by Zumwalt, Cannon, Jenks, Peacock, and Gunning (8), using a liquid nitrogen calorimeter. The results obtained in the present experiment, although similar, were thought to be worth publishing because of the very different techniques involved and the different means of producing the P^{32}.

An aluminum capsule, 0.75 cm. in diameter, 1.02 cm. long, with an average wall thickness of 0.075 cm., was washed in carbon tetrachloride, dried in an oven, and filled with oven-dried red phosphorus. From an analysis of the phosphorus, it was estimated that by allowing a five-day "cooling time" after removal of the sample from the pile, the heat produced by impurities (chiefly Na^{24}) would amount to less than 0.02% of the heat from the phosphorus, and that even the long-lived activities would produce less than 0.02% of the heat for at least the next two months.

The impurities in the aluminum container were not known, so a duplicate empty container was irradiated with the filled one. By monitoring the container filled with phosphorus and the empty container, the phosphorus activity was found to be of the order of 10^4 greater than all activities present in the aluminum. No certain evidence was found from the graph of the decay of the source to indicate that any activity other than P^{32} was present.

The source was inserted in the calorimeter after a "cooling off" period of five days. An approximate bridge balance was obtained about two hours later. Accurate readings of the heat required by the carbon resistor were made twice per day for the following 62 days. These readings, adjusted to noon of each day and corrected for the difference between the observed double deflection of the galvanometer and the double deflections found when the same amount of heat was applied to each calorimeter, are shown in Fig. 6.

The half life of the phosphorus was checked by calculating the disintegration constant over each seven-day interval. The mean value of the half life for the last four weeks differed by 0.4% from the value found for the first four weeks, and the mean value was 14.30 days. The half life reported by Cacciapuoti (1) is 14.30 days ($\pm$0.2%).

The area under the curve was found by summing the daily values of heat output. It may be shown that for $T = 14.3$ days the area found in this way is only 0.01% less than the true integrated area. This method of averaging, which

gives most statistical weight to readings taken when the power produced by the phosphorus was large, was used since the accuracy is best for large values of power. The probable error of any calorimetric reading was approximately constant, amounting to $\pm 0.3\%$ when the readings started, and to $\pm 5\%$ when the phosphorus activity had decayed by a factor of 20. The probable error in the area under the decay curve was 0.1%.

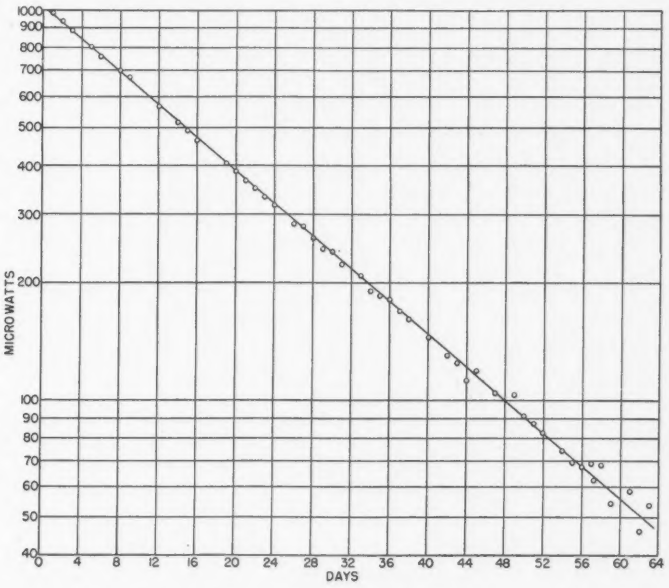

FIG. 6. *Heat produced by* P^{32}.

As a check on the area and its probable error found by taking the sum of the daily power produced, three similar analyses of the data were made by summing every third power reading. This method gave, of course, the same area, and a probable error, based on the dispersion of the three results, of 0.105%.

Bremsstrahlung Correction

The amount of energy lost as bremsstrahlung from the calorimeter was small, since the greater part of the β-ray energy was dissipated in the light elements, aluminum and phosphorus, while the bremsstrahlung had to pass through a silver wall which recovered almost half of it by absorption.

Chien Shuing Wu (7) found that the inner bremsstrahlung produced by P^{32} carries 0.14% of the total disintegration energy, and that the outer bremsstrahlung produced in aluminum carried about 0.57%. These estimates were verified by the writer. Assuming these values and the equivalent spectral dis-

tribution given by Miss Wu and correcting for the bremsstrahlung produced but not absorbed in the phosphorus, aluminum, and silver, it was found that $0.5 \pm 0.2\%$ of the total disintegration energy was lost.

Final Results on P^{32} Source

The final result of the calorimetric measurements showed that the source was producing 47.4 μw. at 2400 February 16, 1949. The error in this value is $\pm 0.4\%$ (Table I).

TABLE I

PROPAGATION OF ERRORS

Measurement of electrical power, %	0.07
Calibration of calorimeter, %	0.2
Prob. error in mean, from dispersion of data, %	0.1
Bremsstrahlung correction error, %	0.2
Uncertainty in half life, %	0.2
Resultant error, % =	0.4

The P^{32} spectrum has been investigated by Siegbahn (5), and Langer and Price (3). The maximum energies found were 1.712 ± 0.008, and 1.689 ± 0.010 Mev. respectively. The spectrum is accurately represented by the Fermi allowed type distribution, at least above 0.1 Mev. (5). The mean energy of disintegration, calculated by assuming this Fermi distribution and taking the maximum energy as the mean of the two values given above, is 0.690 ± 0.004 Mev. Then the disintegration rate at 2400 February 16th, 1949, was 42.9×10^7 disintegrations per second, with a probable error of 0.7%.

The absolute counting result was not available until 0800 March 30, 1949, or 41.33 days later. During this time the source decayed by a factor of 0.1349 ($\pm 0.4\%$), the error resulting from the uncertainty of 0.2% in the half life. The number of disintegrations per second was then 5.78×10^7 ($\pm 0.8\%$).

Twelve measurements of the absolute disintegration rate were made by Mr. R. C. Hawkings. The result was 5.68×10^7 disintegrations per second, with a probable error, based on the dispersion, of $\pm 0.6\%$ and an estimated absolute error of $\pm 2\%$.

Acknowledgments

The writer is indebted to Dr. B. W. Sargent for suggesting this problem and his continuous interest, to Mr. R. C. Hawkings for carrying out the absolute counting with his equipment, and to Mr. T. Hughes for assistance in constructing and operating the calorimeter.

References

1. CACCIAPUOTI, B. N. Nuovo cimento, 15: 213. 1938.
2. GREENWOOD, I. A., HOLDAM, J. V., and MACRAE, D. Mass. Inst. Technol. Rad. Lab. Series, 21: 23. 1948.

3. LANGER, L. M. and PRICE, H. C. Phys. Rev. 76: 641. 1949.
4. RUTHERFORD, E. and ROBINSON, H. Phil. Mag. 25: 314. 1913.
5. SIEGBAHN, K. Phys. Rev. 70: 127. 1946.
6. TIAN, A. J. chim. phys. 20: 132. 1923.
7. WU, CHIEN SHUING. Phys. Rev. 59: 481. 1941.
8. ZUMWALT, L. R., CANNON, C. V., JENKS, G. H., PEACOCK, W. C., and GUNNING, L. M. Science, 107: 47. 1948.

CONTINUOUS OBSERVATIONS WITH THE ELECTRON MICROSCOPE ON THE FORMATION OF EVAPORATED FILMS OF SILVER, GOLD, AND TIN[1]

By T. A. McLauchlan, R. S. Sennett, and G. D. Scott

Abstract

A special specimen holder has been constructed for the evaporation of metals within an RCA–EMU electron microscope. This provides continuous observations on the growth of films of the metal. Micrographs are reproduced which illustrate the formation of films of silver, gold, and tin. The results confirm the usually accepted assumptions regarding the formation of nuclei and the growth of aggregates.

Introduction

It has been established in recent years that metal films thinner than a critical thickness usually consist of a number of aggregates separated by distinct channels. However, little work has been reported on the nature of the aggregates in different films and the process by which they grow to produce the characteristic structure observed at greater thicknesses.

The aggregated structure was first assumed by Faraday (2) in 1857 in order to explain the brilliant colors observed in thin gold films. Similar assumptions were made to explain the variation with thickness in the electrical resistance of the thin films (9). Other workers explained these properties by assuming that the thinner films were continuous and amorphous (11) or by assuming a variation in the mean free path of the conduction electrons (7).

Among the first to report direct observations on the discontinuous structure of thin metal films were Reinders and Hamburger (8) in 1918. They showed, by means of the ultramicroscope, that the particle size in films of a number of metals varied with thickness. Andrade and Martindale (1) studied silver and gold films thicker than 300 Å with a light microscope but observed aggregates only after the films had been heated (at 280°C. for silver and 400°C. for gold). They found that these aggregates became larger on further heating. However, these films were much thicker than the films studied in this work.

X-ray and electron diffraction studies indicate that the metal films in general consist of small crystallites (3). The most conclusive proof was given by electron microscope observations. Numerous workers (6), (5) have reported that the films of a number of metals were aggregated.

In a previous paper from this laboratory (10) an attempt was made to follow the process of formation of metal films from observations made on a series of

[1] *Manuscript received April 12, 1950.*

Contribution from the Department of Physics, University of Toronto, Toronto, Ont. Part of this research was carried out while one of the authors (T. A. M.) was holder of an Ontario Research Council award and another of the authors (R. S. S.) was holder of a National Research Council of Canada award (1948-49). This paper was presented in part at the E.M.S.A. meeting in Washington, October, 1949.

films of gradually increasing thickness. Micrographs were taken which showed the characteristic structure at a number of measured thicknesses, and from these the formation and growth of the aggregates could be inferred. In order to study the changes in individual aggregates, thin metal films have been deposited in the electron microscope so that continuous observations could be made as the film thickness is increased. This procedure eliminates the effects of exposure to air, methods of handling, and aging.

Experimental

A special specimen holder for evaporating the metal was made for the RCA type EMU electron microscope. It is shown in Fig. 1, in which (*a*) is a general view of the holder with the specimen chamber door, and (*b*) is a diagram giving the details of construction of the holder. A V-filament of tungsten wire is inserted in the posts which are mounted in the lucite cap. Four-mil wire was found to be most suitable since it supported the metal satisfactorily but produced little general heating of the holder. The thin brass tube through the cap is connected electrically to the wall of the holder by means of a set screw. Its purpose is to shield the beam, and to prevent evaporated metal from reaching the interior of the microscope. Diaphragming shields inserted above the specimen reduce effects due to metal reflected from the walls of the holder. Flexible formex leads connected the filament to the Kovar seals in the specimen chamber door. The voltage supply was merely a storage battery with a variable resistor.

During an evaporation, the electron beam of the microscope was deflected by the magnetic field of the heating current. A slight displacement of the gun corrected for this deflection and permitted continuous observation throughout the evaporation. However, to obtain good micrographs the evaporation was interrupted at short intervals and the image of the film recorded under steady conditions. Special masks inserted above the photographic plate allowed either 10 or 20 exposures to be taken on one 2 in. × 10 in. plate. In this way a series of micrographs of the same area of the film were obtained at successive stages of the evaporation.

The substrate was in all cases formvar film about 150 Å thick, as normally used for electron microscopy. It has been found (10) that formvar has much the same characteristics as glass when used as a substrate for films of the metals discussed herein.

It is well known that a high intensity electron beam, such as can be obtained in the electron microscope, may increase the aggregation of a metal film. Furthermore, long exposures to a high intensity beam may produce a "contamination" layer over the specimen. To minimize these effects a focusing device similar to that described by Le Poole (4) was constructed. This enabled accurate focusing of the image to be carried out quickly and at very low intensity. Because this intensity is very much less than that which will give observable specimen changes even with long exposures, it is considered that the

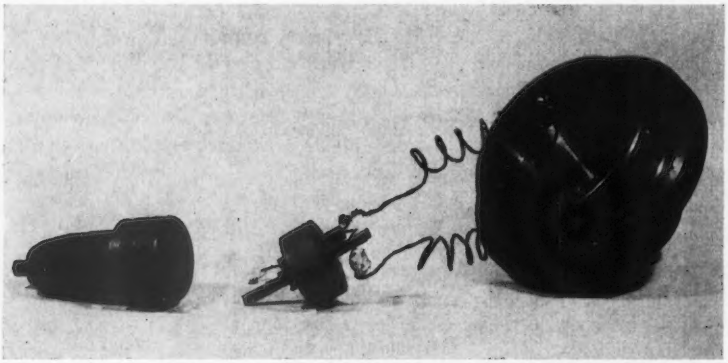

a

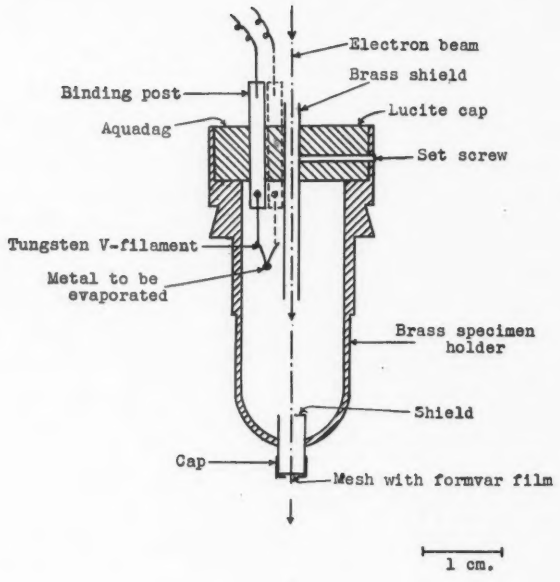

b

FIG. 1. *General view and diagram of the specimen holder for evaporating metals in the microscope.*

electron beam has had no appreciable effect on the films studied in these experiments.

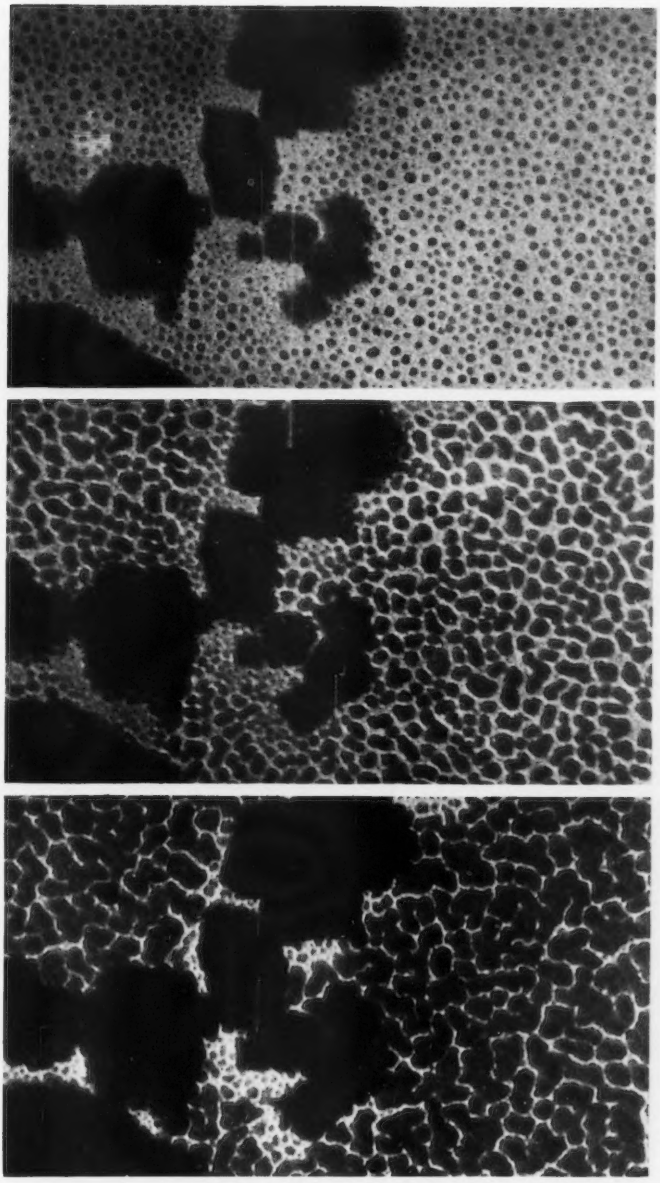

FIG. 2. *Three stages in the formation of an evaporated silver film on a formvar substrate. The magnesium oxide crystals are for identification of the area.* (× 150,000)

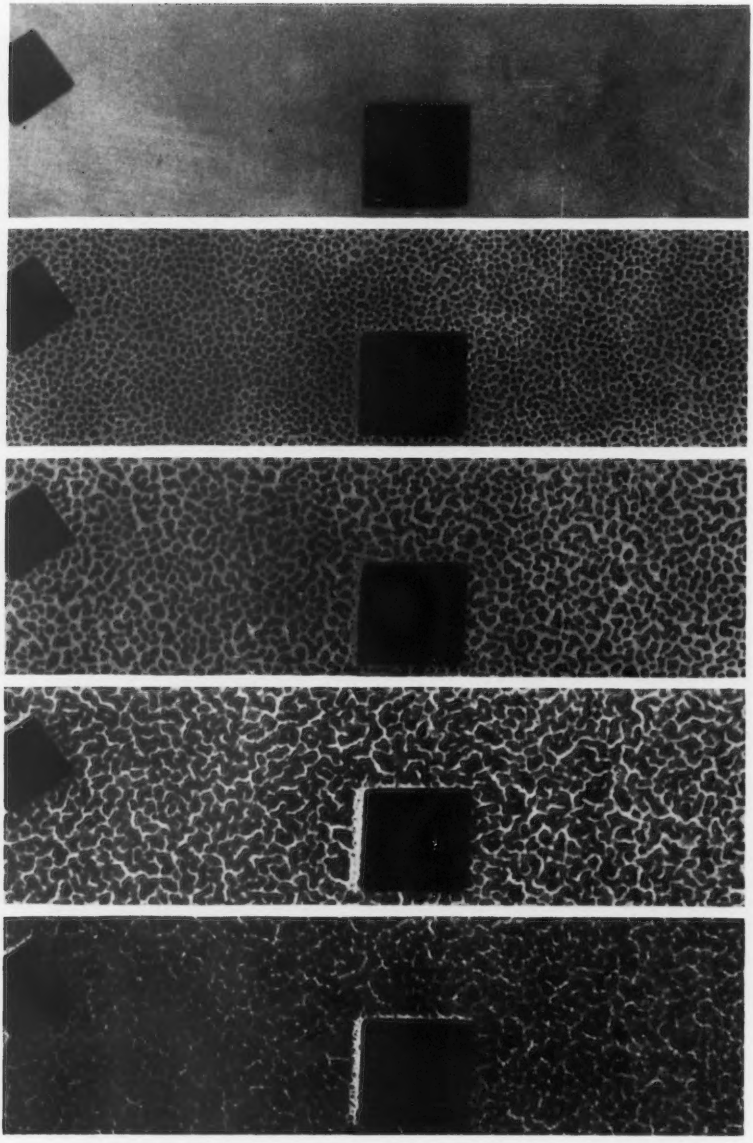

FIG. 3. *The formation of an evaporated gold film.* (× —80,000)

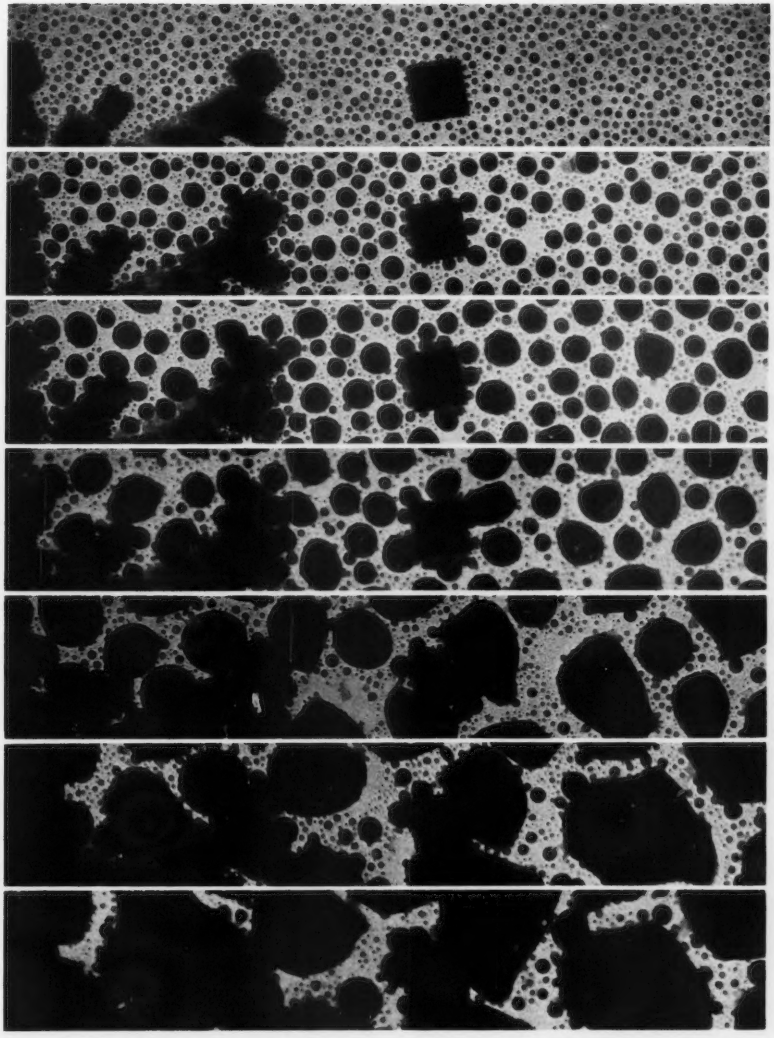

FIG. 4. *The growth of aggregates in a film of tin.* (×—83,000)

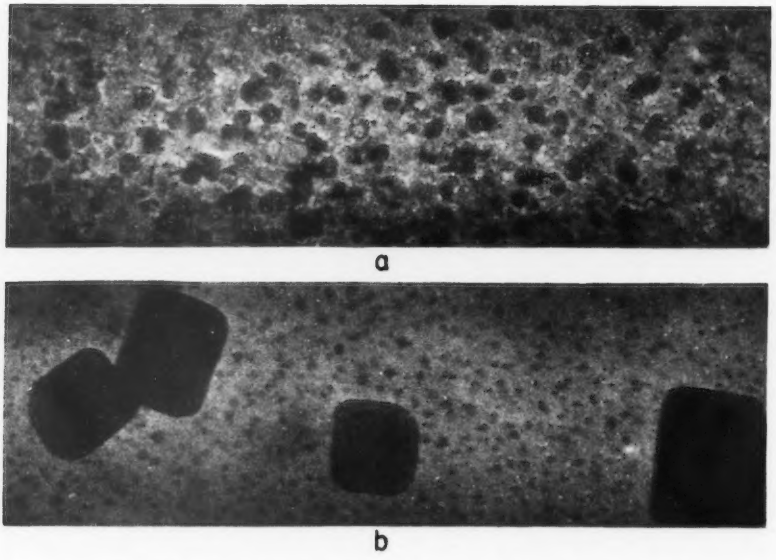

FIG. 5. *Evaporated film of sodium chloride (a) before, (b) after exposure to room air, illustrating the marked recrystallization which occurs in the presence of the air.* (× 90,000)

A series of micrographs showing three steps in the formation of a silver film is given in Fig. 2. The large particles are magnesium oxide crystals which were placed on the formvar prior to the evaporation and which serve to identify the area and the location of individual aggregates. The thicknesses of the films, as judged by comparison of their appearance with silver films of known thickness, are approximately 75 Å, 125 Å, and 150 Å. It can be noted that the film commences as a dispersion of almost spherical globules of various sizes down to the resolution limit of the microscope. The next step shows the merging of the globules into larger aggregates. Although this process is apparently affected by surface tension the aggregates are no longer round, but have become rather irregular in shape. The last stage shows how a further deposition of the metal causes more of the aggregates to unite and leaves only narrow, uniform channels between the remaining aggregates. Although silver has a cubic face-centered lattice there is little evidence of this in the shape of the aggregates. The extent of the migration is illustrated by the aggregates which are formed in the "shadows" of the magnesium oxide crystals even in the thinnest films.

The variations which occur in the formation of a gold film are shown in Fig. 3. The first micrograph is of the plain formvar substrate with magnesium oxide crystals for identification. The succeeding micrographs are of films whose thicknesses are approximately 40 Å, 70 Å, 130 Å, and 190 Å. The general appearances and the changes in structure with increasing thickness appear to be quite similar to those in the silver films.

A tin series is shown in Fig. 4. In the case of this metal, which has a much lower melting point than silver or gold, the aggregation appears to be very greatly affected by surface tension. It should be noted that some of the aggregates, rather than just merging, are actually pulled together so that substrate which was previously covered is left bare. The largest aggregates are beginning to show some angularity.

Though the above metals are not greatly affected by exposure to air, many substances may undergo marked changes in the presence of oxygen or water vapor. An example of such an effect is shown in Fig. 5. A film of sodium chloride was evaporated in the microscope, photographed, then exposed to room air, and finally rephotographed. The original film, Fig. 5, (*a*), exhibits a layer of merged crystallites, whereas after exposure to the air relatively large separate crystals appear on a background of small aggregates. The change is presumably caused by recrystallization in the presence of the water vapor in the air.

Discussion

Appleyard, Lennard-Jones, and others* have discussed the processes by which evaporated atoms of a metal reach their final stable state as a thin film on a substrate. It is to be expected that for gold, silver, and tin, migration

* *Conference on the Conduction of Electricity in Solids, at Bristol. Proc. Phys. Soc. London, 49 (extra part): 151. 1937.*

of the metal atoms over the substrate will be an important factor in the formation of the films.

Our micrographs indicate that for films of these metals migration does in fact lead to the formation of nuclei upon which subsequent atoms collect to form aggregates. The aggregates grow and merge together and very few, if any, new nuclei appear. Appleyard mentions that surface tension may affect the shape of the particles. Such would appear to be the case for these metals.

Another factor which has an important effect on the shape of the aggregates is the rate of evaporation of the metal to form the film. It has been shown for example (10) that with rapid evaporation (two seconds) of a silver film the aggregates grow out as irregular flat platelets to cover the substrate completely at a thickness of about 200 Å, whereas for slow evaporation (20 min.) the aggregates are less irregular and are not as flat so that at an average thickness of 200 Å the film appears highly agglomerated and becomes continuous only when the thickness reaches about 1000 Å. This result suggests that the processes which control the shape of the aggregates such as the action of surface tension, the decay of lattice defects within the aggregate, or the assimilation by the aggregate of newly arrived atoms, take place in finite times and hence are influenced by the rate of additional atoms.

It would appear that considerably more experimental information is required before a quantitative theory of the mechanism of formation of evaporated films can be established. However, the results provide a verification of the assumptions which are usually made in discussing the mechanism and they also confirm the interpretations made from a series of different films of increasing thickness.

References

1. ANDRADE, E. N. and MARTINDALE, J. G. Proc. Roy. Soc. (London), A, 235: 69. 1935.
2. FARADAY, M. Proc. Roy. Soc. (London), A, 147: 145. 1857.
3. GERMER, L. H. Phys. Rev. 56: 58. 1939.
4. LEPOOLE, J. B. Philips Tech. Rev. 9: 33. 1947.
5. LEVINSTEIN, H. J. Applied Phys. 20: 306. 1949.
6. PICARD, R. G. and DUFFENDACK, C. S. J. Applied Phys. 14: 291. 1943.
7. RICHTER, E. Kolloid Z. 61: 208. 1932.
8. REINDERS, W. and HAMBURGER, R. Proc. Kon. Ned. Akad. Wet. 20: 1135. 1918
9. REINDERS, W. and HAMBURGER, R. Ann. Physik, 10: 915. 1931.
10. SENNETT, R. S. and Scott, G. D. J. Optical Soc. Am. 40: 203. 1950.
11. SMAKULA, A. Z. Physik, 88: 114. 1934.

MEASUREMENTS OF GRAVITY IN THE CANADIAN ARCTIC AND GREENLAND[1]

By Michael Beer

Abstract

Four determinations of gravity were made during the summer of 1948, with the pendulum apparatus of the Dominion Observatory, at Goose Bay, Labrador (latitude 53°), Frobisher Bay, Baffin Island (latitude 64°), Resolute Bay, Cornwallis Island (latitude 75°), and Thule, Greenland (latitude 77°), approximately. The anomalies at the two most northerly stations are comparatively small and those at the other two stations, although larger, do not exceed many that have been observed in other parts of Canada. Norgaard's determination at Thule is confirmed by the author.

It is anticipated that these determinations, apart from their immediate interest, will serve as useful reference points for future work in the Canadian Arctic.

Introduction

Determinations of gravity in the Eastern Canadian Arctic and in Greenland were made possible by transportation that became available with an icebreaker during the summer of 1948. The pendulum apparatus of the Dominion Observatory was placed at the disposal of the writer, for the purpose, by the Dominion Astronomer, and a grant to cover expenses was made to the Chairman of the Associate Committee of Geodesy and Geophysics by the National Research Council of Canada.

Apart from the desirability of such determinations to serve as reference points or bases for future work in this great and hitherto more or less inaccessible area, it was thought the results might be of some interest in connection with possible isostatic readjustments following removal of former ice sheets.

The Pendulum Apparatus

This apparatus has been employed by the Dominion Observatory for many years. It is of the Mendenhall type with the knife edge, not on the pendulum, but serving as the support for the pendulum. The pendulum head has the form of an inverted stirrup into which is set an agate plate which rests on the knife edge when the pendulum is in motion. The knife edge is set in a holder of brass which in turn is secured to a shelf in the upper part of the pendulum case. The manner in which observations are taken with it has been described by Klotz (1), McDiarmid (2), and Swick (6).

Temperatures of the pendulums varied from zero at Resolute Bay to 22°C. at Ottawa. Corresponding corrections to the times of vibration of the pendulum

[1] *Manuscript received February 22, 1950.*
Vol. 1, No. 5. Contributions from the Dominion Observatory. Published by permission of the Director, Mines, Forests and Scientific Services Branch, Department of Mines and Resources, Ottawa, Canada.

were made by employing the coefficients determined in 1929 (4). The pendulum case was evacuated to pressures varying from 40 to 60 mm. of mercury and the corresponding corrections were derived from the table on page 90 of Mr. Swick's publication (6).

Chronometer Comparisons and Flexure Correction

Two chronometers adjusted to gain one second in fifty were used to time the pendulums. The rates of these chronometers were determined by comparison with time signals from station WWV at Washington.

The correction due to flexure in the pendulum support has been discussed in previous publications of this Observatory (3, 5) and actual determinations by the interferometer method are described (3). The value of 11×10^{-7} was adopted for all field stations and 10×10^{-7} was adopted for Ottawa. As the apparatus was always set up on a rigid base it is considered, judging from prevous experience with it, that the error in estimating this correction is negligible.

Tabulation and Discussion of Results

The results of all the observations are summarized in Table I, which gives the observed periods of the pendulums at each station and the corresponding deduced values of gravity relative to Ottawa for which the value 980.622 cm. per sec.^{2} was adopted in 1930 following comparison with Potsdam, Greenwich, and Washington in 1929 and 1930.

Differences in the periods of the pendulums observed on each knife edge and also the differences in period on the two knife edges are given for each pendulum in Table II. The extent to which the figures remain constant in each column is a measure of the relative constancy of the times of vibration of the pendulums.

Principal facts including the Free Air and Bouguer anomalies for the four field stations are given in Table III.

Conclusions of a general nature can hardly be drawn from the results for such a small number of stations but a few observations of some interest may, nevertheless, be made.

First, it will be noticed that the Free Air and Bouguer anomalies for each station are not very different, owing of course to the fact that all the stations are little above sea level. Second, it will be observed that the anomalies for the extreme northerly stations are the smallest, not large enough to indicate any great departure from either isostasy or from theoretical gravity as given by the international formula for gravity. The largest observed anomaly is that at the most southerly station, Goose Bay. That anomaly and the one at Frobisher Bay are moderately large, but nevertheless not larger than many that have been observed in other parts of the country.

It is of interest to remark that the writer's observations confirm those of Norgaard's at Thule. Norgaard's station is about one and one half miles north

TABLE I

PENDULUM PERIODS AND DEDUCED VALUES OF GRAVITY

Number and station		No. of swings	Knife edge I			Knife edge II			Mean
			Pendulum			Pendulum			
			1	2	3	1	2	3	
1	Ottawa, (April 16-20, 1948)	8	0.4999778	0.5000857	.....	0.4999745	.....	0.5000602	980.622
			g	.....	.....	.....	.....	.....	
187	Goose Bay, Labrador	12	0.4998006	0.4999100	0.4998893	0.4997975	0.4999064	0.4998852	981.312
			g 981.317	981.312	981.306	981.316	981.312	981.309	
188	Thule, Greenland	10	0.4993918	0.4994999	0.4994779	0.4993881	0.4994971	.....	982.923
			g 982.924	982.923	982.922	982.925	982.920	.....	
189	Resolute Bay, Cornwallis Island	9	0.4994041	0.4995115	.....	.....	.....	0.4994869	982.876
			g 982.876	982.877	.....	.....	.....	982.875	
190	Frobisher Bay, N.W.T.	5	0.4995846	0.4996919	.....	.....	.....	.....	982.167
			g 982.166	982.168	.....	.....	.....	.....	
187	Goose Bay, Labrador	5	0.4998018	0.4999096	.....	.....	.....	.....	981.312
			g 981.311	981.313	.....	.....	.....	.....	
1	Ottawa, (Sept. 14-20, 1948)	12	0.4999775	0.5000854	0.5000635	0.4999738	0.5000820	0.5000604	980.622
			g	.....	.....	.....	.....	.....	

TABLE II

RELATIVE CONSTANCY OF PENDULUMS

Station	Difference in periods of pendulums in units of 1×10^{-7} sec.				Differences in periods of pendulums on knife edges 1 and 2 in units of 1×10^{-7} sec.		
	On knife edge 1		On knife edge 2				
	(Pendulum 1) − (Pendulum 2)	(Pendulum 1) − (Pendulum 3)	(Pendulum 1) − (Pendulum 2)	(Pendulum 1) − (Pendulum 3)	Pendulum 1	Pendulum 2	Pendulum 3
Ottawa 1	−1083	—	—	−858	32	—	—
Goose Bay 1	−1083	−861	−1084	−877	31	36	31
Thule	−1081	−861	—	—	39	28	—
Resolute Bay	−1074	—	—	—	—	—	—
Frobisher Bay	−1073	—	—	—	—	—	—
Goose Bay 2	−1078	—	—	—	—	—	—
Ottawa 2	−1082	−862	−1085	−868	37	34	41

TABLE III

PRINCIPAL FACTS FOR GRAVITY STATIONS

Station		Longitude	Latitude	Elevation, ft.	Theoretical gravity, γ_0	Corrections		Computed gravity		Observed gravity	Gravity anomalies	
No.	Name	° ′	° ′			Elevation	Bouguer	Free Air	Bouguer		Free Air	Bouguer
187	Goose Bay, Labrador	60 25.6	53 19.2	131	981.370	−0.012	−0.008	981.358	981.362	981.312	−0.046	−0.050
188	Thule, Greenland	68 53.5	76 31.5	135	982.939	−0.013	−0.008	982.926	982.931	982.923	−0.003	−0.008
189	Resolute Bay, Cornwallis Island	94 54.8	74 41.2	17	982.859	−0.002	−0.001	982.857	982.858	982.876	0.019	0.018
190	Frobisher Bay, Baffin Island	68 33.3	63 44.8	67	982.206	−0.006	−0.004	982.200	982.202	982.167	−0.033	−0.035

and three tenths of a mile east of our station and his station was at an elevation of 10 ft. compared with 135 ft. for our station. His Bouguer anomaly is 11 milligals compared with 8 milligals obtained by the writer, which is in as good agreement as could reasonably be expected.

FIG. 1. *Gravity station at Resolute Bay indicated by the wooden post in the center of the picture.*

The determinations appear to have been made with sufficient accuracy to provide useful reference points or bases and this may perhaps be their chief value.

Because it is now possible to measure gravity so much more rapidly with modern gravimeters than is possible with the pendulum, the chief value of isolated pendulum determinations is to serve as bases to which gravimeter determinations may be tied or referred. On account of the great distance between Ottawa and the Arctic and the correspondingly large difference in gravity, it is not ordinarily easy to determine the difference of gravity between these places with a gravimeter. Apart from limitations due to the nature of the transportation this difficulty arises chiefly from two sources, the limited range of gravity covered by a gravimeter without resetting and the "drift" of the initial reading of the gravimeter.

Difficulties are also experienced in determining gravity with pendulums, of a nature sometimes difficult to account for. They are not, however, directly related to either distance or range in gravity. In the present instance the internal consistency of the pendulum observations and the agreement with Norgaard's value suggest that reasonable confidence can be placed in the results.

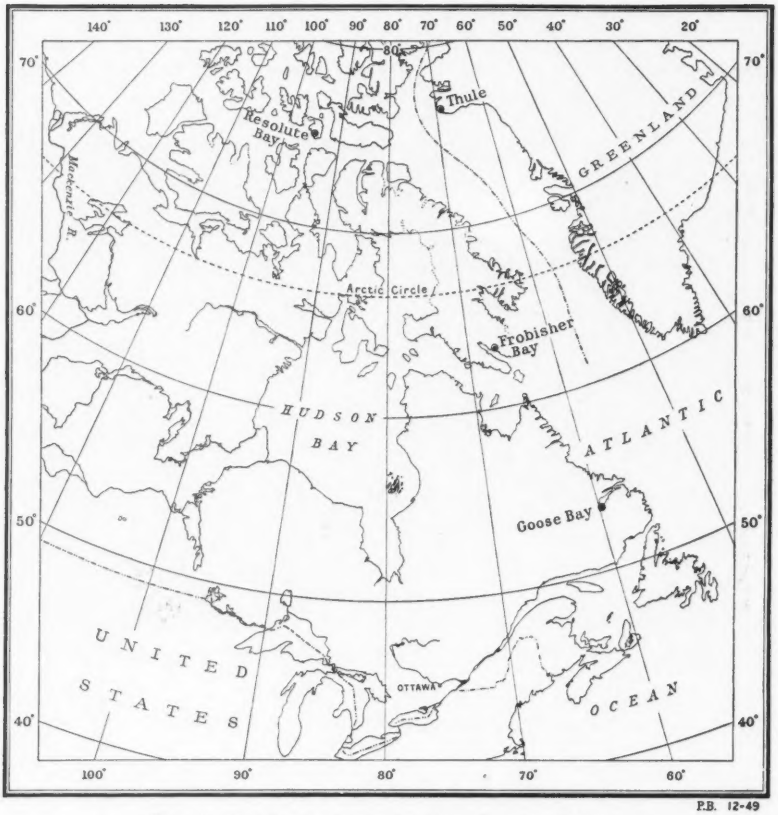

FIG. 2. *Sketch map showing locations of gravity stations.*

Descriptions of Stations

No. 187, Goose Bay, Labrador, (1948)—The apparatus was set up in the east end of the basement of Building No. 20 in the "T" area.

No. 188, Thule, Greenland, (1948)—The apparatus was set up on a granite boulder, about 3 ft. thick, approximately 174 yards on a (true) bearing of 154 degrees from the north lobby of the Danish Magnetic Observatory. Shelter was provided by a structure consisting of wooden crates and boards covered by a heavy canvas.

No. 189, Resolute Bay, N.W.T., (1948)—The apparatus was set up on the rock outcrop in the creek bed south of the meteorological station 1520 ft. from the most northerly transmitting tower on a bearing of 165 degrees and 50 minutes. A shelter was constructed by making use of

the boxes for shipping the apparatus which were held in place by boards. A heavy tarpaulin was placed over and around the boxes, and was held down and protected against the wind by stones and boulders.

No. 190, Frobisher Bay, N.W.T., (1948)—The apparatus was set up in the southwest corner of Building T 82 in the northeast section of the group of buildings in the area.

Acknowledgments

The writer wishes to express his appreciation and thanks to those who made the observations possible by provision of the necessary transportation, including the Royal Canadian Air Force and the staff of the icebreaker. He also wishes to acknowledge his indebtedness to Dr. C. S. Beals, Dominion Astronomer, for making the apparatus available and to his staff for instruction in its use, and to express his thanks to Dr. E. C. Bullard, Professor of Physics, and Dr. J. T. Wilson, Professor of Geophysics, at the University of Toronto, for their encouragement and helpful suggestions.

References

1. KLOTZ, OTTO J. Report on field astronomical observations and description of half-seconds pendulum apparatus. Report of the Chief Astronomer, pp. 24-35. 1905.
2. MCDIARMID, F. A. Pubs. Dominion Observ. 2(10): 201-269. 1915.
3. MCDIARMID, F. A. Pubs. Dominion Observ. 2(10): 236-239. 1915.
4. MILLER, A. H. Pubs. Dominion Observ. 11(2): 62. 1931.
5. MILLER, A. H. and HUGHSON, W. G. Pubs. Dominion Observ. 11(3): 87-88. 1936.
6. SWICK, CLARENCE J. Modern methods for measuring the intensity of gravity. Special publication, No. 69. U.S. Coast & Geodet. Survey. 1921.

PROBABILITY OF AUTO-IONIZATION IN LIGHT ATOMS[1]

By Ta-You Wu and Lorraine Ourom

Abstract

With a view to testing the adequacy of the perturbation theory as applied to radiationless transitions in light atoms, the probability of such a transition in the Be atom from the $1s^2 2p3s\ ^3P$ state to the continuum $1s^2 2s$ + ejected p electron has been calculated. The wave functions employed for the discrete states are obtained by the variational method and the wave function for the continuous state by numerical integration of the Schrodinger equation. The transition probability obtained is 5×10^{13} per second, leading to a width of ~ 290 cm.$^{-1}$ for the level $1s^2 2p3s\ ^3P$. This is at least 10^3 times larger than what is indicated by the observed widths of the spectral lines. Thus the present calculation, together with similar earlier calculations for the He atom, shows that the perturbation theory is inadequate for the light atoms.

It is also pointed out that there is an inconsistency in the use of the perturbation theory in these calculations and those on the Auger effect in the literature since the use of variational or "screened" wave functions implies that a part of the electron–electron interaction has already been included in the initial approximation, and it is hence incorrect to treat this whole interaction as the perturbation causing the transition.

The theory of radiationless transition, such as auto-ionization in optical spectra, Auger effect in X-rays, and predissociation in molecules, is well known. Calculations of the transition probabilities for the Auger effect have been carried out by a number of authors (Burhop (1), Massey and Burhop (3), Pincherle (5)). The results have been found to be in good agreement with the observed "conversion ratios" and the widths of the X-ray lines. For optical spectra, it seems that calculations have been carried out only in the case of the doubly excited states of helium (Wu (7)). The calculated transition probabilities are found to be of the order 10^{14}–10^{15} per second. These large transition probabilities make it difficult to give a satisfactory assignment to the line at 357.5 Å, as the calculated widths of the doubly excited states are too great compared with the observed width of the line. It has been suggested that the perturbation theory treatment of this process may not be adequate, as the transition probabilities are so large (Kiang, Ma, and Wu (2)). The present work is undertaken with the view of making a calculation of the probability of auto-ionization for a case for which a comparison can be made with experimental data.

For this purpose, the Be atom has been chosen. The state for which the probability of auto-ionization has been calculated is the $1s^2 2p3s\ ^3P$ state of BeI. This state goes over to the state $1s^2 2s\kappa p\ ^3P$ in the continuum above the first ionization limit of BeI. Here κp denotes a p electron ejected with the kinetic energy

[1] *Manuscript received May 2, 1950.*
Contribution from the Division of Physics, National Research Laboratories, Ottawa, Canada. Issued as N.R.C. No. 2210.

$$\frac{h^2k^2}{8\pi^2m} = E(1s^2 2p3s\,^3P) - E(1s^2 2s\,^2S).$$

The probability of auto-ionization transition from the initial state, whose wave function is ψ_i, to the final state whose wave function is ψ_f is given by the perturbation theory to be

$$P = \frac{4\pi^2}{h}\left|\int \psi_i^* \frac{e^2}{r_{12}}\psi_f d\tau\right|^2, \tag{1}$$

where the radial wave function for the continuous state κp in ψ_f is normalized in such a way that asymptotically it is given by

$$\frac{1}{r}R_{\kappa p}(r) \to \frac{1}{h}\left(\frac{8\pi m}{k}\right)^{\frac{1}{2}}\frac{\sin(kr+\delta)}{r}. \tag{2}$$

In this way, P is in sec.$^{-1}$

We shall give the result of the calculation here but relegate the details of the calculation to the Appendix. It is found that for the $1s^2 2p3s\,^3P$ state of BeI the value of P is

$$P = 5.5 \times 10^{13}\ \text{sec}^{-1}. \tag{3}$$

This transition probability gives for the lifetime of the $1s^2 2p3s\,^3P$ state the value

$$\tau = \frac{1}{p} \cong 1.8 \times 10^{-14}\ \text{sec}. \tag{4}$$

This value for the lifetime leads, according to the uncertainty principle, to a natural width of the level

$$\Delta E > \frac{h}{2\pi}\frac{1}{\tau} \simeq 290\ \text{cm}^{-1}. \tag{5}$$

Now the following lines arising from transition from the $1s^2 2p3s\,^3P$ state have been observed (Paschen and Kruger (4)): $1s^2 2s3s\,^3S - 1s^2 2p3s\,^3P$, $1s^2 2p^2\,^3P - 1s^2 2p3s\,^3P$, $1s^2 2s3d\,^3D - 1s^2 2p3s\,^3P$. The width ΔE in (5) would lead to a width of these lines of the order 50 Å, which is greater than the observed widths of these by at least a factor of 10^3. Such a large discrepancy cannot be due to numerical inaccuracies of the wave functions employed, since the work of Burhop (1) shows that even the use of plane waves instead of the hydrogenic wave functions for the ejection electron still gives P of the same order of magnitude. The calculated value for the transition probability P is of the same general order of magnitude as those for the doubly excited states of He (Wu (7)) and for the Auger transitions (Burhop (1), Massey and Burhop (3), Pincherle (5)).

The failure of the theory in the case of these light atoms can be traced mainly to the poor approximation obtained by treating the electron–electron interaction $\frac{e^2}{r_{12}}$ as a perturbation when it is of the same order of magnitude as the electron–nucleus interactions $\frac{Ze^2}{r_{12}}$. This situation is similar to the well known

failure of the ordinary perturbation theory to give an accurate value for the energy of the ground state of the helium atom. In the case of the Auger transitions in X-rays for heavier atoms, one may expect the perturbation theory to be better. This is in fact seen from the calculations of Pincherle (5) in which a tendency can be discerned toward a closer agreement between the theory and the experimental data as the nuclear charge Z increases.

It should be pointed out also that a question of consistency arises in the actual calculations reported here and in the literature. The formula (1) for the probability of transition is obtained as follows: For argument's sake, consider a two-electron atom with the Hamiltonian

$$H = H(1) + H(2) + \frac{e^2}{r_{12}}. \tag{6}$$

In the initial approximation, $\frac{e^2}{r_{12}}$ is neglected and the state of the system can be developed in terms of the complete set of states of $H^{(0)} = H(1) + H(2)$. The first approximation for the transition probability P is then given by (1) in which the ψ_i and ψ_f are the states of the initial approximation $H^{(0)}$. In the literature, calculations of P are usually carried out by using for ψ_i and ψ_f wave functions which, instead of the purely hydrogenic wave functions for an atom of nuclear charge Ze, are built up of either variational wave functions containing effective charge parameters or Hartree–Fock functions. Now wave functions ψ_i and ψ_f so constructed do not belong to the complete set of any single Hamiltonian H^{fic} which may be chosen as the initial approximation. Even if they do, their use implies that they have already included a part of the electron–electron interaction $\frac{e^2}{r_{12}}$ (as represented by the screening parameters) in the initial approximation H^{fic} so that the use of $\frac{e^2}{r_{12}}$ in (1) will have overestimated the "perturbation". Instead, P should be given by

$$P = \frac{4\pi^2}{h}\left|\int \psi_i^* \left| H - H^{\text{fic}} \right| \psi_f d\tau \right|^2, \tag{7}$$

where H^{fic} is a fictitious Hamiltonian of which ψ_i, ψ_f are the eigenstates. That reasonable agreement between the theory and the observed data has been found in the calculations of Burhop and Pincherle is probably due to the fact that for Auger transitions involving only the innermost electrons in the heavier atoms, the use of the effective charge instead of Z will only make a small numerical difference.

From Equation (7) it is seen that a much better approximation should be achieved if, instead of products of single-electron wave functions, wave functions can be used which take a better account of the electron–electron interaction in the initial approximation, such as Hylleraas' nonseparable wave functions. In practice, however, this would be exceedingly difficult since this would mean the finding of a complete set of wave functions of this type.

APPENDIX

The ψ_i, ψ_f in (1) are antisymmetrical combinations of one-electron wave functions, namely

$$\psi_i = \frac{1}{\sqrt{4!}}\begin{vmatrix} \psi^+_{1s}(1)\,\psi^-_{1s}(1)\,\psi^+_{3s}(1)\,\psi^+_{2p}(1) \\ \psi^+_{1s}(2)\,\psi^-_{1s}(2)\,\psi^+_{3s}(2)\,\psi^+_{2p}(2) \\ \psi^+_{1s}(3)\,\psi^-_{1s}(3)\,\psi^+_{3s}(3)\,\psi^+_{2p}(3) \\ \psi^+_{1s}(4)\,\psi^-_{1s}(4)\,\psi^+_{3s}(4)\,\psi^+_{2p}(4) \end{vmatrix}, \quad \psi_f = \frac{1}{\sqrt{4!}}\begin{vmatrix} \psi^+_{1s}(1)\,\psi^-_{1s}(1)\,\psi^+_{2s}(1)\,\psi^+_{\kappa p}(1) \\ \psi^+_{1s}(2)\,\psi^-_{1s}(2)\,\psi^+_{2s}(2)\,\psi^+_{\kappa p}(2) \\ \psi^+_{1s}(3)\,\psi^-_{1s}(3)\,\psi^+_{2s}(3)\,\psi^+_{\kappa p}(3) \\ \psi^+_{1s}(4)\,\psi^-_{1s}(4)\,\psi^+_{2s}(3)\,\psi^+_{\kappa p}(4) \end{vmatrix} \tag{8}$$

where the $+$, $-$ signs denote the sign of the Z-component of the spin of the electron. The wave functions ψ's for the bound electron are given then by the following analytical forms where the parameters α, β, γ, δ are determined by the variational method. The radial wave functions multiplied by r are

$$\begin{aligned} R_{1s} &= \sqrt{4\alpha^3}\, r e^{-\alpha r} \\ R_{2s} &= \left(\frac{12\beta^5}{\alpha^2 - \alpha\beta + \beta^2}\right)^{\frac{1}{2}} r\left(1 - \frac{\alpha+\beta}{3}r\right) e^{-\beta r} \\ R_{3s} &= N_{3s}\, r(1 + Ar + Br^2)\, e^{-\gamma r} \\ R_{2p} &= \left(\frac{4\delta^5}{3}\right)^{\frac{1}{2}} r^2 e^{-\delta r}, \end{aligned}$$

where the constants A and B in R_{3s} are so chosen as to make the wave function of $1s^2 3s 2p\ ^3P$ orthogonal to $1s^2 2s 2p\ ^3P$, i.e.,

$$A = -\frac{5\alpha^3 + 2\alpha^2\beta - 3\alpha\beta^2 + 7\alpha^2\gamma - 2\alpha\beta\gamma - 4\alpha\gamma^2 + 8\beta\gamma^2 + 3\beta^2\gamma}{3\,[5\alpha^2 - \beta^2 - 2\alpha\beta - 2\alpha\gamma + 4\beta\gamma]}$$

$$B = \frac{\alpha+\gamma}{12} \cdot \frac{4\alpha^2(\beta+\gamma) - 2\alpha(\beta+\gamma)^2 + \beta\gamma(9\beta - \gamma)}{5\alpha^2 - \beta^2 - 2\alpha\beta - 2\alpha\gamma + 4\beta\gamma}$$

$$N_{3s}^2 = \frac{4\gamma^3}{1 + \dfrac{3A}{2\gamma} + \dfrac{3(A^2+2B)}{\gamma^2} + \dfrac{15\,AB}{\gamma^3} + \dfrac{45\,B^2}{2\gamma^4}}.$$

The wave function for $1s^2 2s 2p\ ^3P$ is obtained by minimizing the following energy integral for this state with respect to the parameters α, β, δ. In the following, energy is in units of the ionization potential of hydrogen, and length in units of the first Bohr radius a of hydrogen.

$$\begin{aligned} E(1s^2 2s 2p\ ^3P) &= 2\,T(1s) + T(2s) + T(2p) + 2\,V(1s) + V(2s) + V(2p) \\ &\quad + F(1s,1s) + 2\,F(1s,2s) + 2\,F(1s,2p) + F(2s,2p) \\ &\quad - G(1s,1s) - G(1s,2p) - G(2s,2p), \end{aligned}$$

where

$$T(1s) = \alpha^2, \quad T(2s) = \beta^2\left(\frac{1}{3} + \frac{2\beta^2}{\alpha^2 - \alpha\beta + \beta^2}\right), \quad T(2p) = \delta^2,$$

$$V(1s) = -2Z\alpha, \quad V(2s) = -Z\left[\beta - \frac{(\alpha-2\beta)\beta^2}{\alpha^2-\alpha\beta+\beta^2}\right], \quad V(2p) = -Z\delta$$

$$F(1s,1s) = \frac{5}{4}\alpha,$$

$$F(1s,2s) = \frac{\alpha\beta}{\alpha+\beta}\left[1 + \frac{(3\alpha+\beta)\beta^3}{(\alpha+\beta)^2(\alpha^2-\alpha\beta+\beta^2)}\right]$$

$$F(1s,2p) = \delta\left[1 - \frac{x^4}{(1+x)^4} - \frac{2x^4}{(1+x)^5}\right], \quad x = \delta/\alpha$$

$$F(2s,2p) = \delta - \frac{\delta z^4}{(1+z)^4} - \frac{\delta z^4}{(1+z)^5(1-y+y^2)}\left[1 - 2y + 3y^2 + \frac{5(y^2-1)}{1+z} + 5\left(\frac{1+y}{1+z}\right)^2\right], \quad y = \alpha/\beta, \quad z = \delta/\beta$$

$$G(1s,2s) = \frac{8\alpha^3\beta^5}{(\alpha+\beta)^5(\alpha^2-\alpha\beta+\beta^2)}, \quad G(1s,2p) = \frac{56\alpha^3\delta^5}{3(\alpha+\delta)^7}$$

$$G(2s,2p) = \frac{4\beta z^5}{(1-y+y^2)(1+z)^7}\left[14 - \frac{98}{3}\left(\frac{1+y}{1+z}\right) + \frac{185}{9}\left(\frac{1+y}{1+z}\right)^2\right], \quad y = \alpha/\beta, \quad z = \delta/\beta.$$

The wave function of $1s^2 3s 2p\ ^3P$ is obtained by minimizing the energy integral of this state with respect to the parameters α, γ, δ.

$$\begin{aligned} E(1s^2 3s 2p\ ^3P) = {} & 2T(1s) + T(3s) + T(2p) + 2V(1s) + V(3s) + V(2p) \\ & + F(1s,1s) + 2F(1s,3s) + 2F(1s,2p) + F(3s,2p) \\ & - G(1s,3s) - G(1s,2p) - G(3s,2p), \end{aligned}$$

where

$$T(3s) = \frac{N^2}{4\gamma}\left[1 + \frac{A}{\gamma} + \frac{A^2}{\gamma^2} + \frac{3AB}{\gamma^3} + \frac{9B^2}{2\gamma^4}\right]$$

$$V(3s) = -\frac{N^2 Z}{2\gamma^2}\left[1 + \frac{2A}{\gamma} + \frac{3(A^2+2B)}{2\gamma^2} + \frac{6AB}{\gamma^3} + \frac{15B^2}{2\gamma^4}\right]$$

$$\begin{aligned} F(1s,3s) = {} & \frac{N^2}{2\gamma^2}\left[1 + \frac{2A}{\gamma} + \frac{3(A^2+2B)}{2\gamma^2} + \frac{6AB}{\gamma^3} + \frac{15B^2}{2\gamma^4} - \frac{\gamma^2}{(\alpha+\gamma)^2}\right. \\ & \left(1 + \frac{2A+\alpha}{\alpha+\gamma} + \frac{3}{2}\frac{(A^2+2B)+2A\alpha}{(\alpha+\gamma)^2} + 3\frac{2AB+(A^2+2B)\alpha}{(\alpha+\gamma)^3}\right. \\ & \left.\left. + \frac{15}{2}\frac{B^2+2AB\alpha}{(\alpha+\gamma)^4} + \frac{45}{2}\frac{B^2\alpha}{(\alpha+\gamma)^5}\right)\right] \end{aligned}$$

$$\begin{aligned} F(3s,2p) = {} & \frac{N^2}{2\gamma^2}\left[1 + \frac{2A}{\gamma} + \frac{3(A^2+2B)}{2\gamma^2} + \frac{6AB}{\gamma^3} + \frac{15B^2}{2\gamma^4} - \frac{\gamma^3}{(\gamma+\delta)^2}\right. \\ & \left(1 + \frac{4A+3\delta}{2(\gamma+\delta)} + \frac{3}{2}\cdot\frac{A^2+2B+3A\delta+\delta^2}{(\gamma+\delta)^2}\right. \end{aligned}$$

$$+3\cdot\frac{2AB+\frac{3}{2}(A^2+2B)\delta+2A\delta^2+\frac{\delta^3}{3}}{(\gamma+\delta)^3}$$

$$+\frac{15}{2}\cdot\frac{B^2+3AB\delta+(A^2+2B)\delta^2+\frac{2}{3}A\delta^3}{(\gamma+\delta)^4}$$

$$+\frac{45}{2}\cdot\frac{\frac{3}{2}B^2\delta+2AB\delta^2+\frac{A^2+2B}{3}\delta^3}{(\gamma+\delta)^5}$$

$$+\frac{7\times 45}{4}\frac{B^2\delta^2+\frac{2}{3}AB\delta^3}{(\gamma+\delta)^6}+7\times 15\frac{B^2\delta^3}{(\gamma+\delta)^7}\Bigg)\Bigg]$$

$$G(1s,3s)=\frac{10a^3N^2}{(a+\gamma)^5}\left[1+\frac{5A}{a+\gamma}+\frac{3}{5}\frac{11A^2+28B}{(a+\gamma)^2}+\frac{231}{5}\frac{AB}{(a+\gamma)^3}+\frac{837}{10}\frac{B^2}{(a+\gamma)^4}\right]$$

$$G(3s,2p)=\frac{14\delta^5N^2}{3(\gamma+\delta)^7}\left[1+\frac{7A}{(\gamma+\delta)}+\frac{185A^2+414B}{14(\gamma+\delta)^2}+\frac{15\times 111\,AB}{14(\gamma+\delta)^3}+\frac{4\times 13\times 45}{7}\frac{B^2}{(\gamma+\delta)^4}\right],\quad \text{where } N=N_{3s}.$$

Rigorously speaking, the wave function of $1s^23s2p\ ^3P$ should be orthogonal to the wave functions of all the states $1s^22snp\ ^3P$ for all n. In practice, such a calculation would be impossible. As the $2s$ wave function in $1s^22snp\ ^3P$ will probably not vary very much for different values of n, and as the $3s$ wave function in $1s^23s2p\ ^3P$ has already been orthogonalized with the $2s$ wave function in $1s^23s2p\ ^3P$, it is hoped that the error arising from the lack of exact orthogonality of $1s^23s2p\ ^3P$ to all $1s^22snp\ ^3P$ will not be too serious. In fact, it is found that the energy $E(1s^23s2p\ ^3P)$ so calculated does lie above the observed value, so that it really has not sunk below the real eigenvalue on account of this lack of exact orthogonality.

For the final state ψ_f, the wave function of $1s^22s\ ^2S$ has already been calculated by the same method before, and the result is quoted in Table I (Wu (6)). For the continuous wave function of the ejected p electron, the wave equation is the differential–integral equation for the motion of a p electron in the field of the nucleus and the $1s^22s$ electrons, including the effect of exchange,

$$\frac{d^2R_{\kappa p}}{dr^2}+\left[k^2+\frac{2Z}{r}-2V_{1s}(r)-V_{2s}(r)-\frac{2}{r^2}\right]R_{\kappa p}=-G(1s,\kappa p)R_{1s}(r)-G(2s,\kappa p)R_{2s}(r),$$

where

$$V_{1s}(r) = \frac{2}{r}\int_0^r R_{1s}^2(\rho)d\rho + \int_r^\infty \frac{2}{\rho} R_{1s}^2(\rho)d\rho$$

$$V_{2s}(r) = \frac{2}{r}\int_0^r R_{2s}^2(\rho)dp + \int_r^\infty \frac{2}{\rho} R_{2s}^2(\rho)d\rho,$$

$$G(1s, \kappa p) = \frac{1}{3}\left[\frac{2}{r^2}\int_0^r \rho R_{1s}(\rho) R_{\kappa p}(\rho)d\rho + r\int_r^\infty \frac{2}{\rho^2} R_{1s}(\rho)R_{\kappa p}(\rho)d\rho\right]$$

$$G(2s, \kappa p) = \frac{1}{3}\left[\frac{2}{r^2}\int_0^r \rho R_{2s}(\rho) R_{\kappa p}(\rho)d\rho + r\int_r^\infty \frac{2}{\rho^2} R_{1s}(\rho) R_{\kappa p}(\rho)d\rho\right].$$

The equation is integrated numerically by a process of successive approximation (Wu (7)). The probability P in sec.$^{-1}$ of auto-ionization of the state $1s^2 3s2p\ ^3P$ to $1s^2 2s\kappa p\ ^3P$ is given by (1) in which the wave functions ψ_i and ψ_f are given by (8). It can be shown, however, that on account of the orthogonality of the $1s$ and the $2s$, $3s$, κp electrons, the $1s^2$ electrons contribute nothing to the transition probability, and in the actual calculation, one can treat the problem as a two-electron system so that

$$\psi_i = \frac{1}{\sqrt{2}}\left|\psi_{3s}(1)\psi_{2p}(2) - \psi_{3s}(2)\psi_{2p}(1)\right|$$

$$\psi_f = \frac{1}{\sqrt{2}}\left|\psi_{2s}(1)\psi_{\kappa p}(2) - \psi_{2s}(2)\psi_{\kappa p}(1)\right|.$$

On carrying out the integration over the angles, the integral in (1) becomes

$$\left|\int \overset{*}{\psi}_i \frac{1}{r_{12}} \psi_f d\tau_1 d\tau_2\right|^2 = \left|\iint R_{3s}(1) R_{2s}(1) \frac{1}{r_>} R_{2p}(2)R_{\kappa p}(2)\, dr_1 dr_2 - \frac{1}{3}\iint R_{3s}(1) R_{\kappa p}(1) \frac{r_<}{r_>^2} R_{2p}(2)R_{2s}(2)dr_1 dr_2\right|^2.$$

These integrals are readily calculated by graphical integration.

The result of the calculations is given in the following tabulation.

Be	α	β	γ	δ	E_{calc}	E_{obs}(in Rhc)
$1s^2 2s^2 S$	3.69	1.365			−28.520	−28.642
$1s^2 2s2p^3P$	3.69	1.20		0.90	−28.965	−29.152
$1s^2 3s2p^3P$	3.69	1.20	0.5	1.05	−28.392	−28.572

$P(1s^2 3s2p\ ^3P — 1s^2 2s\kappa p\ ^3P) = 5.5 \times 10^{13}$ per second.

References

1. Burhop, E. H. S. Proc. Roy. Soc. (London), A, 148: 272. 1935.
2. Kiang, A. T., Ma, S. T., and Wu, T. Y. Chinese J. Phys. 2: 117. 1936.
3. Massey, H. S. W. and Burhop, E. H. S. Proc. Roy. Soc. (London), A, 153: 661. 1936.
4. Paschen, F. and Kruger, P. G. Ann. Physik, 8: 1005. 1931.
5. Pincherle, L. Nuovo Cimento, 12: 81. 1935.
6. Wu, T. Y. Phil. Mag. 22: 837. 1936.
7. Wu, T. Y. Phys. Rev. 66: 291. 1944.

CANADIAN JOURNAL OF RESEARCH

Notes on the Preparation of Copy

GENERAL:—Manuscripts should be typewritten, double spaced, and the **original and one extra copy** submitted. Style, arrangement, spelling, and abbreviations should conform to the usage of this Journal. Names of all simple compounds, rather than their formulae, should be used in the text. Greek letters or unusual signs should be written plainly or explained by marginal notes. Superscripts and subscripts must be legible and carefully placed. Manuscripts should be carefully checked before being submitted, to reduce the need for changes after the type has been set. If authors require changes to be made after the type is set, they will be charged for changes that are considered to be excessive. **All pages, whether text, figures, or tables, should be numbered.**

ABSTRACT:—**An abstract of not more than about 200 words, indicating the scope of the work and the principal findings, is required.**

ILLUSTRATIONS:

(i) *Line Drawings:*—All lines should be of sufficient thickness to reproduce well. Drawings should be carefully made with India ink on white drawing paper, blue tracing linen, or co-ordinate paper **ruled in blue only**; any co-ordinate lines that are to appear in the reproduction should be ruled in black ink. Paper ruled in **green, yellow, or red should not be used** unless it is desired to have all the co-ordinate lines show. Lettering and numerals should be neatly done in India ink preferably with a stencil (**do not use typewriting**) and be of such size that they will be legible and not less than one millimeter in height when reproduced in a cut three inches wide. All experimental points should be carefully drawn with instruments. Illustrations need not be more than two or three times the size of the desired reproduction, but the ratio of height to width should conform with that of the type page. **The original drawings and one set of small but clear photographic copies are to be submitted.**

(ii) *Photographs:*—Prints should be made on glossy paper, with strong contrasts; they should be trimmed to remove all extraneous material so that essential features only are shown. Photographs should be submitted **in duplicate;** if they are to be reproduced in groups, one set should be so arranged and mounted on cardboard with rubber cement; the duplicate set should be unmounted.

(iii) *General:*—**The author's name, title of paper, and figure number should be written in the lower left hand corner (outside the illustration proper) of the sheets on which the illustrations appear.** Captions should not be written on the illustrations, but typed on a separate page of the manuscript. All figures (including each figure of the plates) should be numbered consecutively from 1 up (arabic numerals). **Each figure should be referred to in the text.** If authors desire to alter a cut, they will be charged for the new cut.

TABLES:—Titles should be given for all tables, which should be numbered in Roman numerals. Column heads should be brief and textual matter in tables confined to a minimum. **Each table should be referred to in the text.**

REFERENCES:—**These should be listed alphabetically by authors' names, numbered in that order, and placed at the end of the paper.** The form of literature citation should be that used in the respective sections of this Journal. **Titles of papers should not be given in references listed in Sections A, B, E, and F, but must be given in references listed in Sections C and D.** The first page only of the references cited in papers appearing in Sections A, B, and E should be given. **All citations should be checked with the original articles.** Each citation should be referred to in the text by means of the key number; in Sections C and D the author's name and the date of publication may be included with the key number if desired.

Reprints

Fifty reprints of each paper without covers are supplied free. Additional reprints, if required, will be supplied according to a prescribed schedule of charges. On request, covers can be furnished at cost.